TELECOMMUNICATIONS ENGINEERING SCHOOL
TECHNICAL UNIVERSITY OF CARTAGENA

MASTER THESIS
MASTER'S DEGREE IN TELECOMMUNICATION ENGINEERING

Investigations in coupled cavity systems for searching dark matter axions

Author: Pablo Navarro Martínez
Advisor: Alejandro Melcón Álvarez
Co-advisor: Antonio José Lozano Guerrero

Author	Pablo Navarro Martínez
Author's e-mail	pablonm.ct.94@gmail.com
Project advisor	Alejandro Álvarez Melcón
Project advisor's e-mail	alejandro.alvarez@upct.es
Project co-advisor	Antonio José Lozano Guerrero
Project co-advisor's e-mail	Antonio.Lozano@upct.es
Title of the Master's Thesis	Investigations in Coupled Cavity Systems for Searching Dark Matter Axions
Abstract	The aim of the project consists of the realization of investigations of coupling cavity structures [1] for a searching system of dark matter axions [2]. This main goal will be divided into three particular objectives. The first one consists of the evaluation of periodic cavity's structures. The second one is the study of the characteristic and behaviour of a structure with couplings with alternating sign. Finally, the third goal will be based on exploring the possibilities of introducing a tunable system for searching axions.
Degree	Master's Degree in Telecommunications Engineering
Department	Information Technologies and Communications
Date of submission	May 2019

II

Acknowledgements

I would like to express my sincere gratitude to my master's thesis advisors Antonio José Lozano Guerrero and Alejandro Álvarez Melcón for their continuous support and for answering all my doubts.

Furthermore, I am deeply grateful to the whole RADES team, which contributes to accomplish this project both at personal and professional levels.

Thanks to everybody for giving me the opportunity to join the team.

Contents

List of Figures

List of Tables

1   Introduction

1.1   Axions

Axion is a hypothetical particle which appears in formulations in order to explain a standard model problem, called the strong CP problem. In particle physics, CP-symmetry is the combination of Charge conjugation symmetry (C-symmetry) and parity symmetry (P-symmetry). Peccei and Quinn [3] [4] proposed a solution to this problem, by introducing anomalous global symmetry. It was soon realized that such a solution to the strong CP problem leads to a light pseudo scalar particle : the axion.

Axion is a neutral, stable and very light particle. It interacts weakly with conventional matter. Due to this interaction, we can classify the experiments focused in searching axions in two main groups:

Axion helioscope : this experimental searches for the axion are based on the interactions with two photons. As a consequence of this interaction, axions can transform into photons and vice-versa under strong electric and magnetic fields. This process takes place in stars, where axions are produced through the transformation of thermal photons in the presence of electric field. Our closest star is, evidently, the sun, becoming in our brightest source of axions. As it an be observed in figure 1 Solar axions streaming from the sun would be reconverted into photons in the presence of a transverse electromagnetic field in a laboratory.
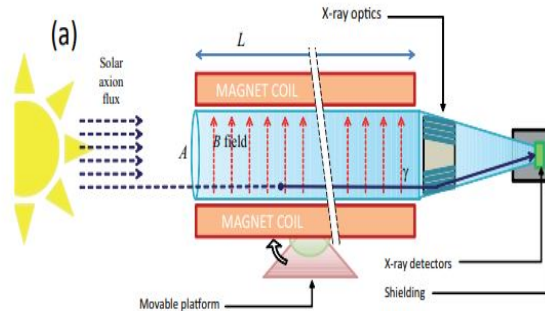
Figure 1: Schematic of a solar axions experiment

Axion haloscope : Axion haloscopes try to detect dark matter (DM) axions in the galaxy by using microwave cavities. Under a strong magnetic field, the axion DM may produce radio wave with its frequency corresponding to the axion mass, and it is amplified if the size of the cavity matches with the axion's wavelength. Note that this technique crucially relies on the assumption that the observed DM consists of cold axion.

The conventional axion haloscope technique [5] consists of a high-Q microwave cavity inside a magnetic field to trigger the conversion of axions from our galactic DM halo into photons. Being non-relativistic, the axions convert to monochromatic photons with energy proportional to its mass. For a cavity whose resonant frequency matches that specific energy, and consequently, to the mass, the conversion is enhanced by a factor proportional to the quality factor of the cavity Q. For a high Q cavity, the resonant band is small and thus the cavity must be tunable and data taking is performed by scanning very thin mass-slices of parameter space.
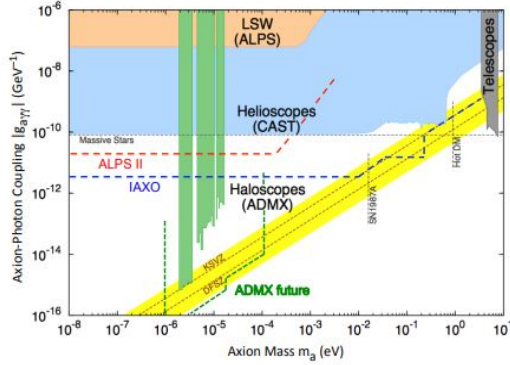
Figure 2: Schematic of the theoretical axion mass range of different axion experiments

Since its prediction four decades ago, there has not been any evidence for its discovering. Nevertheless, the efforts have not decayed, in fact, the number of experiments have grown up significantly. So far the most relevant experiments are ADMX, CASPEr and CAST [2] [6] [4]. It is expected a new generation of helioscope with IAXO (International Axion Observatory). Figure 2 shows the different ranges of mass and energy that are being explored for searching axions.

1.2 Axion Searches with Microwave Filters:The RADES Project

In this project, we design and construct a variant of the conventional axion haloscope concept that could be competitive in the search for dark matter axions of masses in the decade $10 - 100\mu eV$. Theses masses are located somewhat above the mass range in which existing experiments have reached sensitivity to benchmark quantum chromodynamic (QCD) axion models. Our haloscope consists of an array of small microwave cavities coupled by rectangular irises, in an arrangement commonly used in radio-frequency filters.

The size of the unit cavity determines the main resonant frequency, while the possibility to connect a large number of cavities allows to reach large detection volumes. We develop the theoretical framework of the detection concept, and present design prescriptions to optimize detection capabilities.

We describe the design and realization of various small-scale prototypes of this concept, called Relic Axion Detector Exploratory Setup (RADES). It consists of a copper-coated stainless steel five-cavities microwave system with the detecting mode operating at around 8.4 GHz. This structure has been electromagnetically characterized at 2 K and 298 K, and it is now placed in ultra-high vacuum in one of the twin-bores of the 9 T CAST (CERN Axion Solar Telescope) dipole magnet at CERN (European Organization for Nuclear Research) 3. We describe the data acquisition system (DAQ) developed for relic axion detection, and present preliminary results of the electromagnetic properties of the microwave system, which show the potential of coupling cavities systems to reach QCD axion window sensitivity at X-band frequencies.

Figure 3: Image of dipole magnet CAST located at CERN

1.3 Description of the project

In the under graduate thesis [7], we showed the behaviour of a six cavities filter, the procedure to obtain it by using a theoretical physic model as well as how we make the data taking process. Once we have understood the behaviour of this small prototype, the next step consists on the design and manufacturing of a larger and more complex structure of searching axions. In order to obtain this structure, we have divided the project in three main sections:

[I] **Theoretical model**: First of all, we should review some theoretical concepts and relevant parameters previous to the main part of the project.

[II] **Very long structures with periodic conditions**: Simulating very large structures with a huge amount of resonant cavities could be really time consuming. As far as time is concerned, applying periodic boundary conditions could be a good

solution for our project. In this chapter we will introduce the theoretical concept and how we can design a microwave filter by using this concept.

[III]**Alternated coupling cavity**: Since we have designed and studied a five cavities filter with inductive irises, the next step consists of the study of more complex structures. For doing that, we are going to simulate a filter with capacitive irises. Afterwards we are going to develop a filter with both irises, inductive and capacitive, alternating in the same system. We will do a study for each structure.

[IV] **A mechanical tunable cavity**: In this chapter we are going to elaborate a mechanical tunable system for searching axions. The challenge of this part is to create a system with a great frequency range variation but without losing any of its properties.

1.4   Software used in this project

1.4.1   CST Microwave Studio

CST Microwave Studio (CST MWS) is an electromagnetic simulation software specialised in 3D simulations of high frequency components.

CST MWS enables the fast and accurate analysis of high frequency devices such as antennas, filters, couplers, etc.

1.4.2   Matlab

MATLAB (Matrix laboratory) is a multi-paradigm numerical computing environment which allows matrix manipulations, plotting of functions and data, implementation of algorithms, etc.

2 Theoretical model

Taking into account [2], we can describe the figure of merit or F.O.M, which determines the quality of our device for searching axions, as follows in equation 1:

$$F.O.M. = g_{A\gamma}^4 m_A^2 B^4 V^2 T_{sys}^{-2} C^4 Q \tag{1}$$

where B is the magnetic field (assumed constant over the cavity volume), V is the cavity *volume*, T corresponds with the noise temperature, and C and Q are respectively, the geometrical and quality factors of the cavity resonant mode. The main objective of this project consists in maximising the F.O.M. The magnetic field is given by an external dipole magnet and it can not be modified, so the only feasible ways of increasing the figure of merit is by the C and Q factors and the cavity volume.

2.1 Loaded and Unloaded Q

The quality factor Q is a measure of the losses of a resonant circuit. It is defined as the relation between the energy stored in our system and the power loss. the quality factor depends directly on the capacity of the resonator for storing energy. On the other hand, The greater losses our system have, the lower Q we get. If we apply this relationship to a resonator of lumped elements formed by an inductor and a capacitor:

$$Q = \omega \frac{(average\ energy\ stored)}{energy\ loss/second} = \omega \frac{W_m + W_e}{P_l} \tag{2}$$

where W_m is the average magnetic energy stored in the capacitor and W_e is the average electric energy stored in the inductor.

$$W_m = \frac{1}{4}|I|^2 L \tag{3}$$

$$W_e = \frac{1}{4}|V_c|^2 C = \frac{1}{4}|I|^2 \frac{1}{\omega^2 C} \tag{4}$$

Due to the fact that any resonant circuit is invariably coupled to other external circuit, which will modify the global quality factor, we have to distinguish between the intrinsic conditions of our system and those external condition that affect our system.

The quality factor Q defined in the absence of any loading effects caused by external circuitry is called the unloaded Q or Q_u. When we include the effects of external systems we obtain the loaded Q or Q_L. The Q_L is obtained as:

$$\frac{1}{Q_L} = \frac{1}{Q_u} + \sum \frac{1}{Q_e} \tag{5}$$

If we consider that our resonant circuit is not affected by any external loading effect, then $Q_L = Q_u$. Note that in any other case Q_L will be smaller than Q_u. In order to calculate the optimum value of Q_L of the experiment [2] we have to match our Q_u with the combination of all the external effects Q_e.

$$\frac{1}{Q_u} = \sum \frac{1}{Q_e} \tag{6}$$

The non trivial simplest case is when we have a structure with just one port, then it is easy to see that $Q_u = Q_e$ and $Q_L = \frac{Q_u}{2}$. However, when the number of ports increases, then the optimum value of Q_L is when $Q_u = \sum Q_e$, but the relation between Q_u and Q_L keeps unaltered, which means that the more amount of ports we have in our system, the less coupled they must be in order to keep an optimum Q_L.

When the value of the combination of external quality factors is higher than Q_u, then our system is said to be over-coupled. On the other side, if Q_u is higher, it is said to be under-coupled.

There are several forms of calculating the different quality factors of a microwave filter. Additionally, we can obtain easily either the loaded or external quality factors through the Scattering parameters. For a two ports filter, We can calculate Q_e of each port from the S_{ii} parameter and the Q_l factor from the S_{ij} parameter. In the case of the Q_L we will use equation 7.

$$Q = \frac{f}{BW} \tag{7}$$

Where f is the resonant frequency of the resonator mode and BW corresponds with the *bandwidth*, in this case of 3 dB, of the same resonator.

2.2 Critical coupling

To obtain maximum power transfer between a resonator and a feedline, the resonator must be matched to the feed at the resonant frequency. Then we can say that the resonator is critically coupling to the feed.

It is useful to define a coupling coefficient, g as:

$$g = \frac{Q_u}{Q_e} \tag{8}$$

There are three cases which can be distinguished:

I $g < 1$ The resonator is said to be undercoupled to the feedline.

II $g = 1$ The resonator is critically coupled to the feedline.

III $g > 1$ The resonator is overcoupled to the feedline.

2.3 Cavity coupling

According to M.Pozar [8], the coupling factor between two cavities can be described as the ratio among the coupled and stored energy introduced by a coupling element.

$$k = \frac{\iiint \varepsilon E_1 E_2 \, dv}{\sqrt{\iiint \varepsilon |E_1|^2 dv \times \iiint \varepsilon |E_2|^2 dv}} + \frac{\iiint \mu H_1 H_2 \, dv}{\sqrt{\iiint \mu |H_1|^2 dv \times \iiint \mu |H_2|^2 dv}} \tag{9}$$

The coupling factor can be obtained from the electric and magnetic field, where E_i represents the electric field of the specific cavity and H_i its magnetic field ($i = 1, 2$). ϵ ans μ are the permittivity and permeability respectively. In the right side of the equation, the first element represents the electric coupling whereas the second represents the magnetic coupling.

Then, if we use capacitive couplings, we obtain a positive k whereas in inductive couplings the k factor is negative. The only restriction to use these equations is that both resonant cavities must be identical. If not, to extract the coupling factor, the expression 9 must be employed, using the electromagnetic field inside the cavities.

2.4 Form factor C

The form factor C is a measure of how the electric field of a resonant mode of a cavity is aligned with an external magnetic field. It can be calculated as:

$$C = \frac{\left(\int dV \, E_{cav}(x) B_0(x) \right)^2}{V |B_0|^2 \int dV \, \epsilon(x) E_{cav}^2(x)} \tag{12}$$
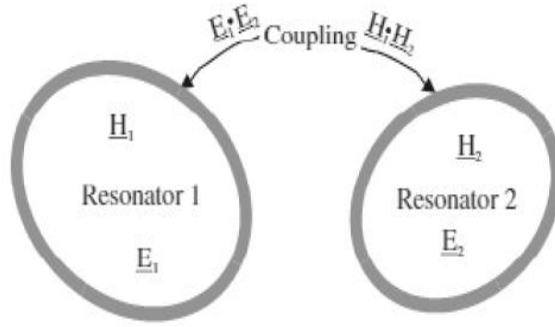
Figure 4: General view of a coupling between two radiofrequency resonators, M.Pozar [8]

A positive value in the coupling factor means that the energy stored in the resonators is increased due to the coupling. On the other side, a negative value implies a reduction in the energy stored. Due to that fact, we can associate a positive value with a capacitor and a negative to a inductor

As we described in [7], an alternative way of calculating both, the electric and magnetic coupling factor, is through the even (f_e) and odd (f_o) frequencies applying symmetries. The equations to be used are the following:

$$k_E = \frac{f_e^2 - f_o^2}{f_e^2 + f_o^2} = \frac{C_m}{C} \tag{10}$$

$$k_M = \frac{f_o^2 - f_e^2}{f_e^2 + f_o^2} = \frac{L_m}{L} \tag{11}$$

Due to the direct relation between the electric field in the cavity and the C factor. At first glance, it seems obvious that the simplest and more logical solution would be working with the first resonant mode, which presents a positive electric field in the whole structure. If we align the electric cavity field with the external one, the C factor must be the maximum possible. However, as we showed in [7], there are some issues that makes this kind of systems infeasible. Following the idea described in [7], we are going to optimize this factor, designing more complex structures in which the phase mode is not the first.

2.5 Theoretical model for a multi cavity filter

In this project, we cannot use directly an identical resonant cavities system in which all of them resonate at the same specific frequency. We need to use a mathematical model

that maximise the C and Q values. For doing so, we are going to use the following matrix which represent a coupling cavities system

$$\Omega = \begin{pmatrix} \Omega_1^2 & K_{12} & 0 & 0 & 0 & 0 \\ K_{12} & \Omega_2^2 & K_{23} & 0 & 0 & 0 \\ 0 & K_{23} & \Omega_3^2 & K_{34} & 0 & 0 \\ 0 & 0 & \ddots & \ddots & \ddots & 0 \\ 0 & 0 & 0 & \ddots & \ddots & \vdots \\ 0 & 0 & 0 & 0 & K_{N-1,N} & \Omega_N^2 \end{pmatrix} \tag{13}$$

where Ω_i is the resonant frequency of the i-th cavity when it is isolated, and $K_{i,i+1}$ is the

coupling factor normalised between the i-th cavity and (i+1)-th. It is a square matrix of size NxN in which we will have N different eigenvalues λ_i associated to this matrix that represent the natural frequency of the coupling cavities system. Each eigenvalue will have associated an eigenvector which represents the electric field distribution of the specific resonant mode.

In order to maximise the form factor C, we are looking for an eigenvalue in which all the components of the eigenvector will present exactly an equal normalised value of $\frac{1}{\sqrt{N}}$. That will be the mode which couples to axions. Due to the fact that the rest of eigenvectors must be orthonormal to the mode we are looking for, they will not interact with axions and their form factor must be very small ($C \simeq 0$).

Now we are going to solve the eigenvalue problem associated to this matrix. To proceed, we have to enforce the eigenvalue and their corresponding eigenvector as

$$\lambda \begin{pmatrix} x_1 \\ x_2 \\ x_3 \\ \vdots \\ x_N \end{pmatrix} = \Omega \begin{pmatrix} x_1 \\ x_2 \\ x_3 \\ \vdots \\ x_N \end{pmatrix} = \begin{pmatrix} x_1\Omega_1^2 + x_2 K_{12} \\ x_1 K_{12} + x_2\Omega_2^2 + x_3 K_{23} \\ x_2 K_{23} + x_3\Omega_3^2 + x_4 K_{34} \\ \vdots \\ x_{N-1}K_{N-1,N} + x_N\Omega_N^2 \end{pmatrix} \tag{14}$$

Where x_i are the components of the eigenvector associated to the eigenvalue λ.

Substituting $K_{i-1,i} = k_{i-1,i}\lambda$ in equation (14)

$$for \ i = 1 \qquad \lambda = \frac{x_1\Omega_1^2}{x_1 - x_2 k_{12}} \tag{15}$$

$$for \ i \ \in [2, \ N-1] \qquad \lambda = \frac{x_i\Omega_i^2}{x_i - x_{i-1}k_{i-1,i} - x_{i+1}k_{i,i+1}} \tag{16}$$

$$for \ i = N \qquad \lambda = \frac{x_N\Omega_N^2}{x_N - x_{N-1}k_{N-1,N}} \tag{17}$$

As we can observe, at first glance the system is unapproachable due to the huge amount of variables. In order to make it simpler, we are going to stablish the next procedure:

I We stablish the value of the eigenvalue as well as each value of the eigenvector. Depending on the frequency we want, we will choose the eigenvalue. In the case of the eigenvector, we will select a value of $(1, 1, 1, 1, ..., 1)$ for maximising the form factor C.

II We also choose the value of the coupling factor $k_{i,i+1}$ which will correspond with a feasible value to be implemented with inductive or capacitive irises.

III From the equation described previously we are capable of obtaining the different Ω_i values. Then we will have the resonant frequency of each isolated cavity.

IV We have to calculate the physical dimension of each cavity when it is coupled. We just have to calculate the loading effects of each coupling into nearby cavities.

V Probably, a final optimization process is required to compensate for nearby interactions.

3 Very long structures with periodic conditions

3.1 Theoretical concept

According to [8], we can describe periodic structures as an infinite transmission line or waveguide periodically loaded with reactive elements. Periodic structures have a similar response to conventional filters, there are pass and banned bans which determines whether a wave can propagate or not . Typically, it is used in travelling-wave tubes, masers, phase shifters and antennas.

In order to understand the basic wave propagation phenomena associated with periodic structures, we are going to use the simplest example made of infinite repetitions of lumped elements, as shown in figure (5).
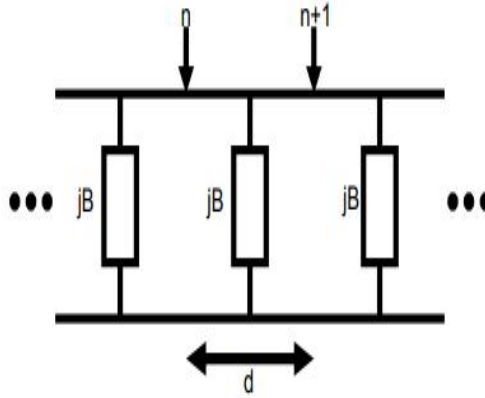
Figure 5: Schematic of a periodic structure formed by lumped elements

We can imitate the procedure described by [8] and [9] by considering a unit cell as a two port network, then the relationship between the input and output ports could be described, using the transmission parameters or ABCD, as:

$$\begin{bmatrix} V_n \\ I_n \end{bmatrix} = \begin{bmatrix} A & B \\ C & D \end{bmatrix} \begin{bmatrix} V_{n+1} \\ I_{n+1} \end{bmatrix} \tag{18}$$

where

$$A = cos\theta - (B/2)sin\theta$$
$$B = j(B/2cos\theta + sin\theta - B/2)$$
$$C = j(B/2cos\theta + sin\theta + B/2)$$
$$D = cos\theta - B/2sin\theta$$

Note that,if we apply the condition for passive networks, then $AD - BC = 1$. Additionally, the electrical length θ could be obtained as $\theta = kd$, where k is the wave number and d is the length of the period.

The next step consists of assuming that our periodic structure is infinitely long, so that the conditions at the input of the n cell must be identical to the (n+1) cell except for a phase delay. The relationship can be described as:

$$\begin{bmatrix} V_n \\ I_n \end{bmatrix} = e^{-\gamma d} \begin{bmatrix} V_{n+1} \\ I_{n+1} \end{bmatrix} \tag{19}$$

As we know, $\gamma = \alpha + j\beta$ and it is the complex propagation constant of the whole periodic structure. Applying the relationship between (18) and (19), the eigenvalue equation is obtained as follows:

$$\begin{bmatrix} A & B \\ C & D \end{bmatrix} = \begin{bmatrix} e^{-\gamma d} & 0 \\ 0 & e^{\gamma d} \end{bmatrix} \tag{20}$$

The non trivial solution is:

$$cosh\gamma d = cos\theta - b/2sin\theta \tag{21}$$

Since the right hand side is purely real, either α or β must be zero. In our first case ($\alpha = 0$), we have a non attenuating structure, in which a wave is propagating along the system and defines the bandpass zone of the structure. In the second case ($\beta = 0$) the wave does not propagate but it is attenuated. It defines the stopband zone of the line.

When we are studying the stopband and passband characteristic of a periodic structure, it is useful to plot the propagation constant β versus the propagation constant of the unloaded line k. Such graph is called a k-β graph, or more commonly, a Brillouin diagram. The k-β diagram can be plotted from the relation shown in equation (21), which is the dispersion relation for a general periodic structure. Independently of its applications for periodic structures, this diagram can be used to study the dispersion characteristic of many types of microwave components. For example, we can consider the dispersion relation for a waveguide mode giving the well known equation

$$\beta = \sqrt{k^2 - k_c^2} \tag{22}$$

3.2 Applications and results

In our previous experiment, we designed a five cavities microwave filter in which the first resonant mode was at 8.4 GHz. The next step consists of creating a new structure with higher volume. In order to get that, we are going to increase the number of cavities of our array. Due to the increase in simulation time with the volume, the analysis of

Parameter	Physical dimension (mm)
a	22.86
b	10.16
$L_1 = L_5$	26.68
$L_2 = L_3 = L_4$	25
W	8
t	2

Table 1: Physical dimensions of the five cavities filter.

the whole structure is practically infeasible. However, the analysis of a infinite periodic structure can be reduced to the analysis of only a period by using periodic conditions.

Firstly, we are going to imitate the behaviour of our first design using periodic conditions, we can observe the geometry of the structure and the resonant modes in figure (6) and table (1) respectively. In this case, one period of the structure consists in one cavity with the same dimensions than the internal cavities of the structure shown in figure 6. However, the coupling length has been reduced from t to t/2 with the aim of defining the period of the corresponding infinite periodic structure.
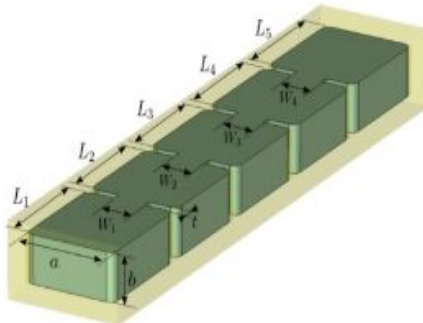

Figure 6: Schematic of the five cavities microwave filter used in the RADES experiment [2]

The periodic structure and its dispersion curve are represented in figure (7) and figure (8) respectively. The period of this structure are composed by one resonant cavity and the coupling among cavities, in this case we use half coupling in each side of a cavity. Note that in the case of the periodic cavity, instead of having any discrete resonant frequency, we are able to calculate a continuous dispersion diagram for a particular phase of the periodic conditions. Theoretically, if we have a structure with infinite cavities, the first mode of this system corresponds with the frequency obtained at 0 degrees of the dispersion curve represented in figure (8). As we only have designed a small structure with 5 cavities, the first and last mode are not located at 0 and 180 degrees of our dispersion curve respectively.

Resonant Mode	Frequency (GHz)	Q
Mode 1	8.445308	7016.1
Mode 2	8.500021	7340.8
Mode 3	8.577578	7628.9
Mode 4	8.658225	8040 1
Mode 5	8.719438	8448.1

Table 2: Resonant frequencies and Q factors for each mode of the inductive irises cavity.
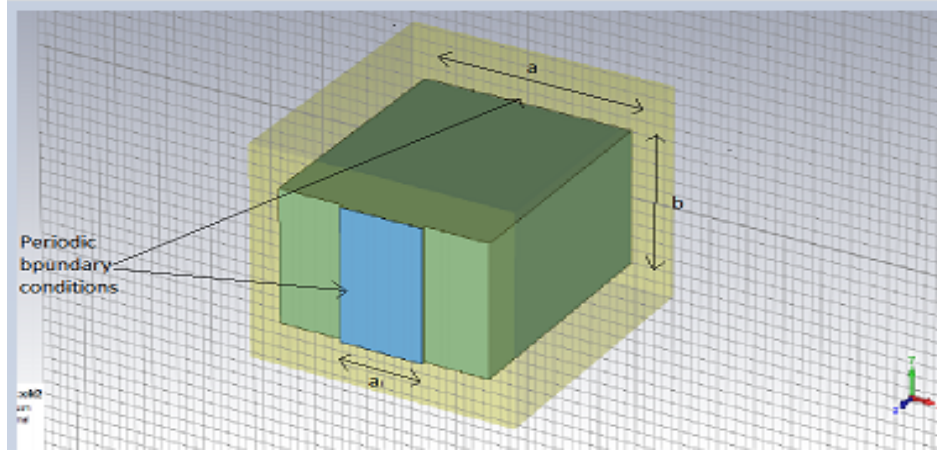

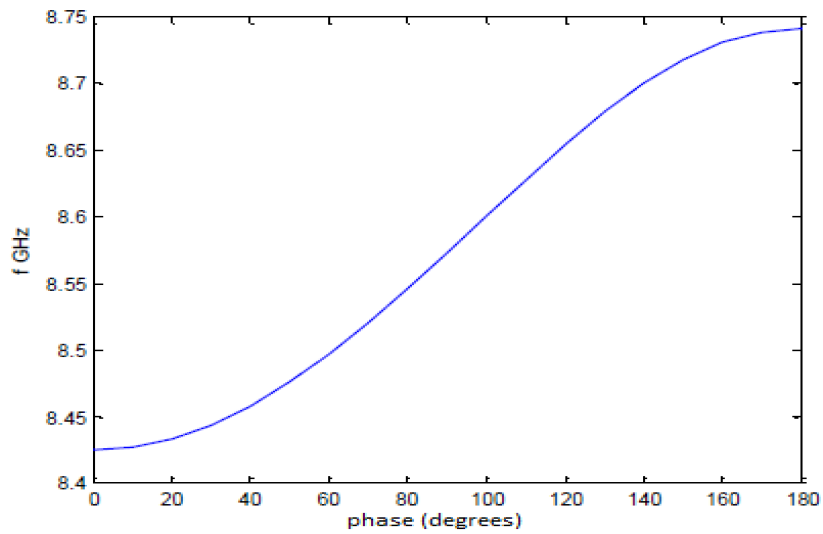Figure 7: Schematic of one cavity period applying periodic boundary conditions

Figure 8: Frequency dispersion curve of an infinite periodic structure applying different periodic condition phases to the unit cell of the periodic structure

Now we are going to study the behaviour of the periodic structure modifying the iris sizes, changing only the width W of both with 1 mm steps. In figure (9), we can

observe the frequency dispersion curves for different values W of the inductive irises. Note that as we increase the width W of the irises, the slope of the curve increases as well as the whole frequency range decreases.

The decrease in the frequency range is caused because, when the iris width W increases, the loading coupling effect increases in the resonator. The increase in the slope means that the frequency resonances will breaking away if the system is finite. Additionally, the slope is smaller at the beginning and the end of the phase range, which means that the resonant frequencies that are located in the limits will be quite close, whereas those frequencies that are in the middle will be more separated.
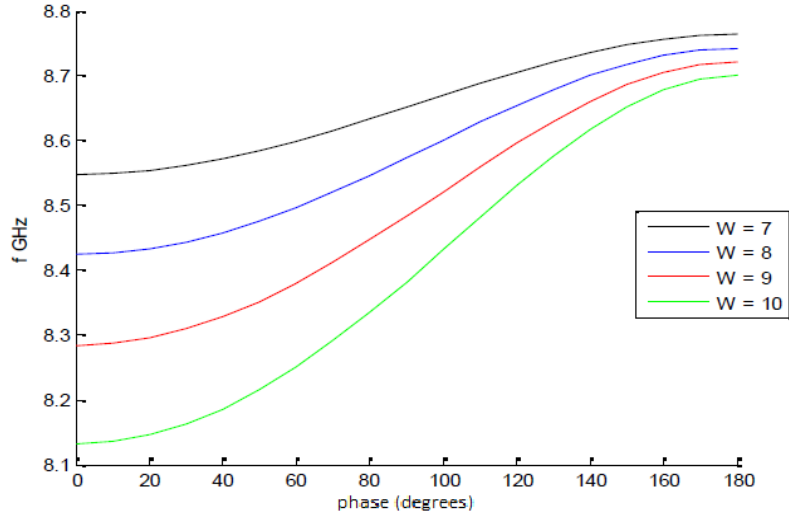

Figure 9: Frequency dispersion curve vs phase of the infinite periodic structure for different values of W with steps of 1 mm

It could be difficult to compare the slope of each curve, so we can eliminate the "offset" of every function in order to compare just the increment of the slope. The increment of frequency generated from the coupling is not an important problem because the length of the cavity can be modified to adjust the resonant frequency. The comparison between the four dispersion curves, when the offset is eliminated, is shown in figure (10).

We have studied the most simple case of periodic structures. The next step is a more complex structure, such as a biperiodic structure. In that case, the unit cell is composed by two cavities and the coupling between them. The cavities are coupled by one of the couplings as we can observe in figure (11). In this case, if the length of both cavities are identical, we are in the same situation than the previous case, in which a period is formed by only one cavity and the coupling. If we want to take advantage of this kind of structures, we should use different length L for each cavity.

When we increase the period of the structure to two cavities like in figure (11), we have a split in the frequency dispersion curve, obtaining two dispersion curves, one for
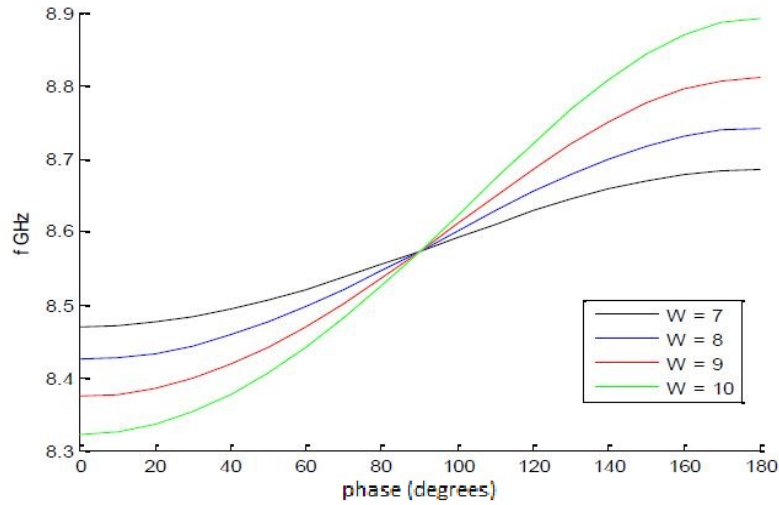
Figure 10: Comparison of dispersion curve among structures with different values of W removing the frequency offset.
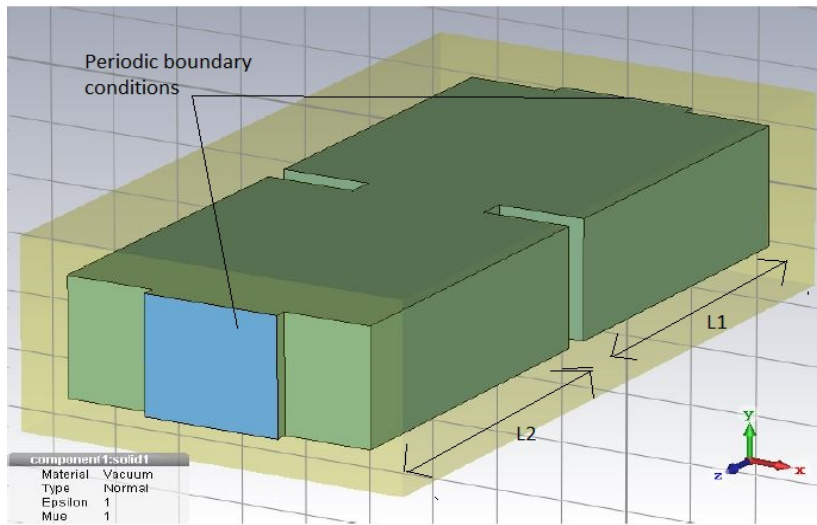

Figure 11: Schematic of a periodic unit cell composed by two cavities coupled with an inductive

each cavity. The separation among the curves, usually called stopband or bandgap, will depend mainly on two factors: the length's difference between the cavities and the width difference among the irises, both the external irises and the one which couples the two cavities. In figure (12) it is represented the dispersion frequency curve for different values of the internal iris (W2) and external irises (W1). The slope of both curves will depend on the difference between the irises width. The frequency split increases as the difference between both widths is higher. As we said before, in the condition W1=W2 (c) we do not have any split because we are in the same situation as in the first periodic structure studied.

16

If we modify the length of the cavities instead of the iris width, we have a similar situation than the previous one. As we can observe in figure (13), the frequency split increases as the length difference between both cavities increases.

We have studied a very simple case such as the first periodic structure and the behaviour of a biperiodic system altering different dimensions of the cavities. Now, the next step consists of designing a more complex structure. We are going to design a periodic unit cell composed by five resonant cavities. Due to we want to design a unit cell with five cavities, each cavity must have a different length. The physical dimensions of the five cavities of one period are showed in table (3). We will make a comparison between the periodic structure and a five cavities system using the same physical dimensions, it is showed in figure (14)

| Parameter	value (mm)
W	8
L1	26.68
L2	25.63
L3	28.43
L4	26.082
L5	26.6

Table 3: Physical dimensions of the unit cell composed by 5 resonant cavities

Applying the theoretical model described in equation 13, the eigenvector obtained in the design of the five cavities system is (1,1,-1,0.6,0.7) which has also a period of 5.

In figure (15), we are seeing a comparison between the five dispersion curves obtained from the periodic structure and the five resonant modes simulated from the five cavities filter. Each mode of the discrete structure corresponds with one dispersion curve of our periodic structure. On the other hand, the slope of the dispersion curves decreases with the period of the periodic structure. Additionally, the band gap among curves is too small for our application, doing the design infeasible.

3.3   Pros and cons of periodic structures

The benefits of working with periodic structures are mainly two: A faster simulation as compared to very long systems (e.g. analysis of 1 period instead of 20 or even more cavities), and the occasion of seeing the whole dispersion curve. On the other hand, the most important problem of working which periodic structures is that we are considering an infinite system. We will have to study more techniques in order to consider the external cavities for a finite system.
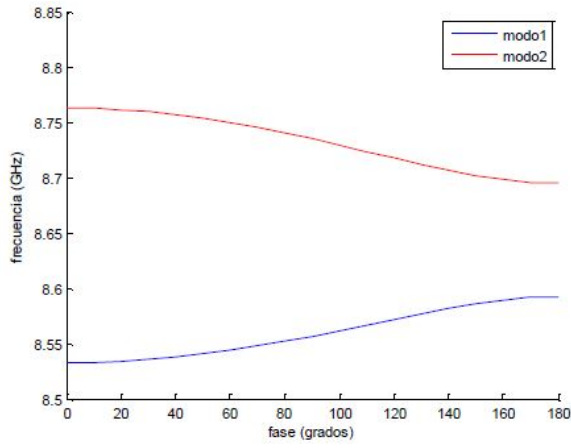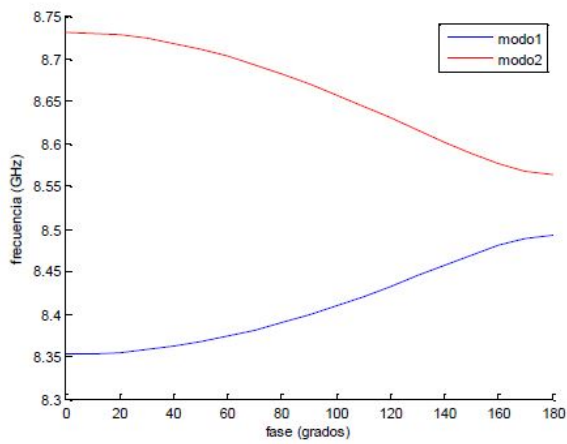
(a) W1 = 8 mm W2 = 6 mm
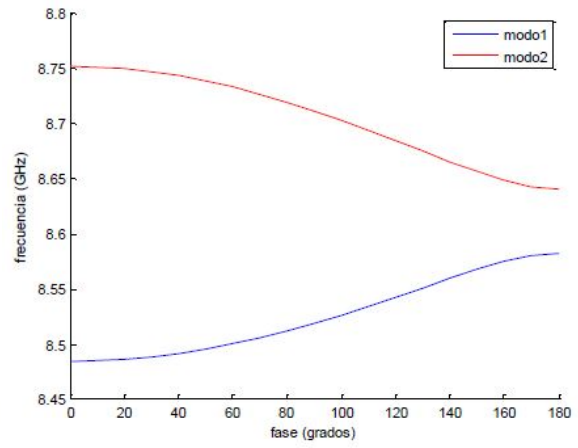
(b) W1 = 8 mm W2 = 7 mm
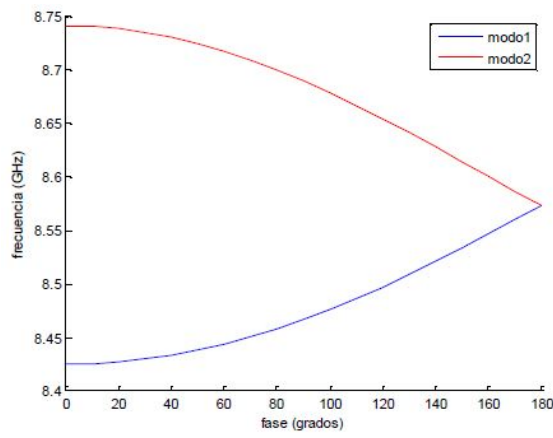
(c) W1 = 8 mm W2 = 8 mm

(d) W1 = 8 mm W2 = 9 mm
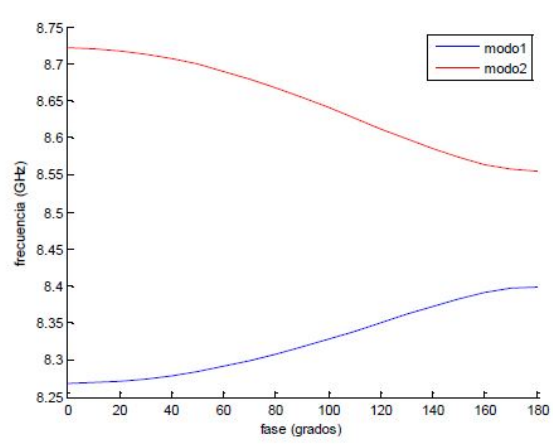
(e) W1 = 8 mm W2 = 10 mm

Figure 12: Comparison of the split in the dispersion curve using different values of W
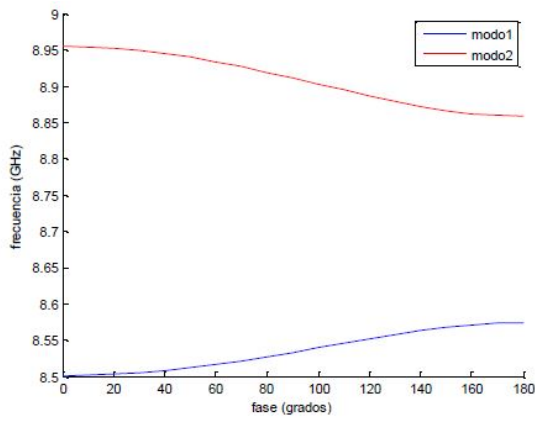
(a) L1 = 25 mm L2 = 23 mm
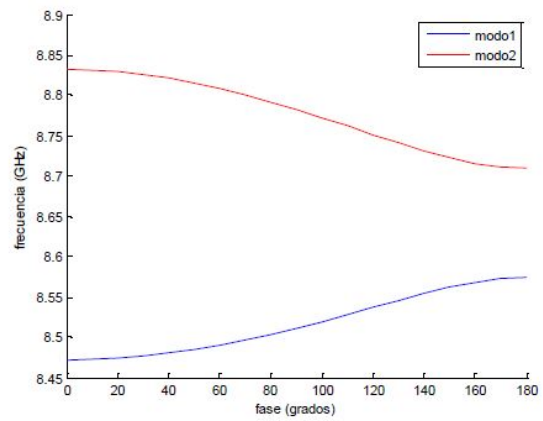
(b) L1 = 25 mm L2 = 24 mm
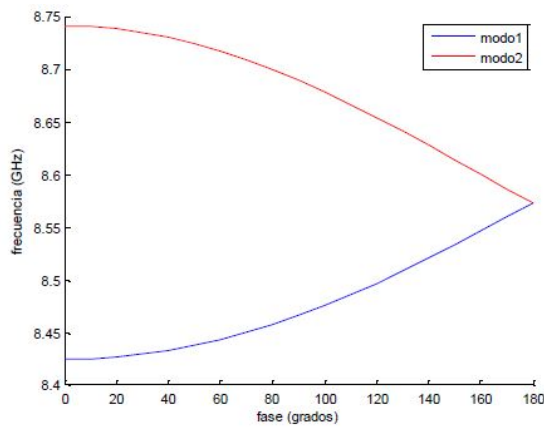
(c) L1 = 25 mm L2 = 25 mm
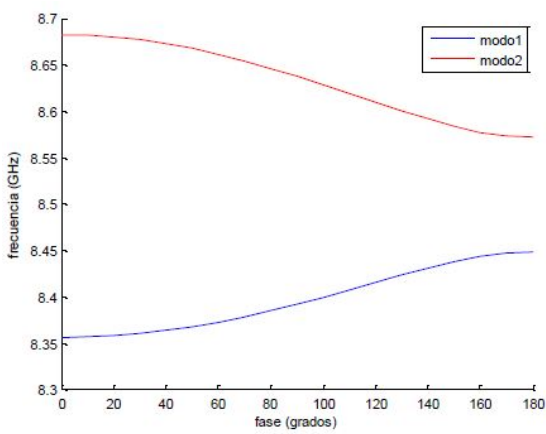
(d) L1 = 25 mm L2 = 26 mm
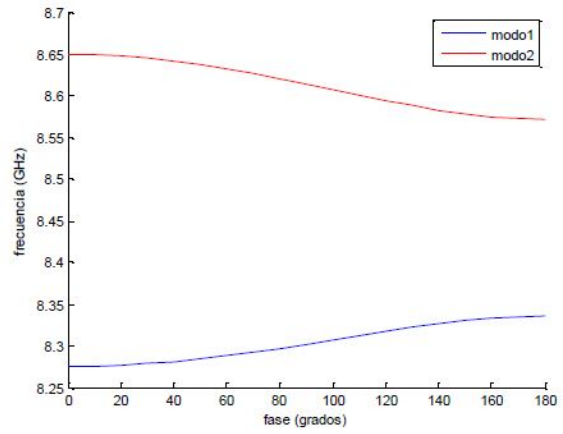
(e) L1 = 25 mm L2 = 27 mm

Figure 13: Comparison of the split in the dispersion curve using different values of L
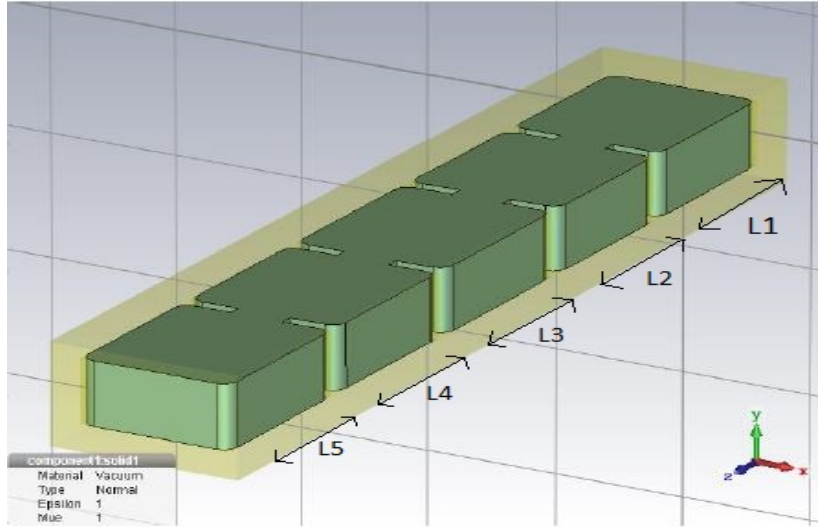
Figure 14: Schematic of a unit cell composed by five different cavities applying periodic boundary conditions
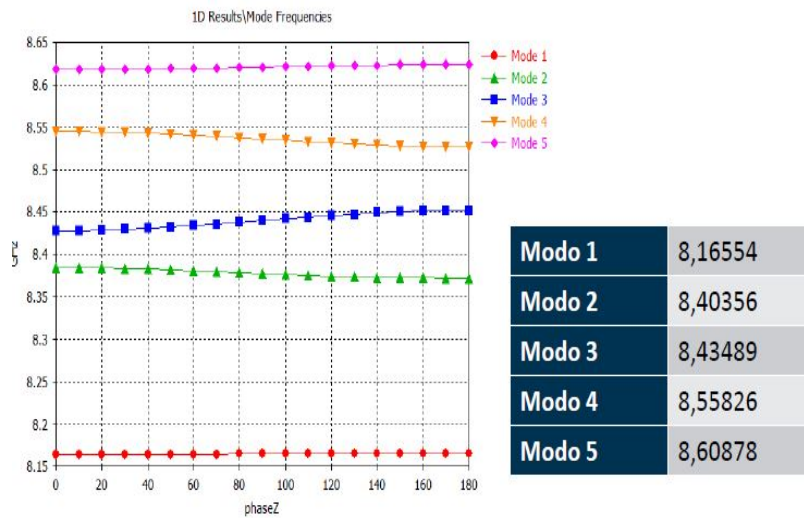
Figure 15: Comparison between the dispersion diagram of a unit cell composed by 5 cavities (left) and a real system of five resonant cavities (right)

4 Alternated coupling cavities

In this section, we are going to develop a resonant cavity system with alternating couplings. We will analyse the mathematical model as well as study the design in simulations and take some measurements in a laboratory.

4.1 Design of different structures

First of all, we have to calculate the k-factor (**??**) for inductive coupling. Once we get it, we should find the k-factor with same value than the inductive coupling but with opposite sign. As we showed in equation (**??**), we can express the electric k-factor by even and odd frequencies.
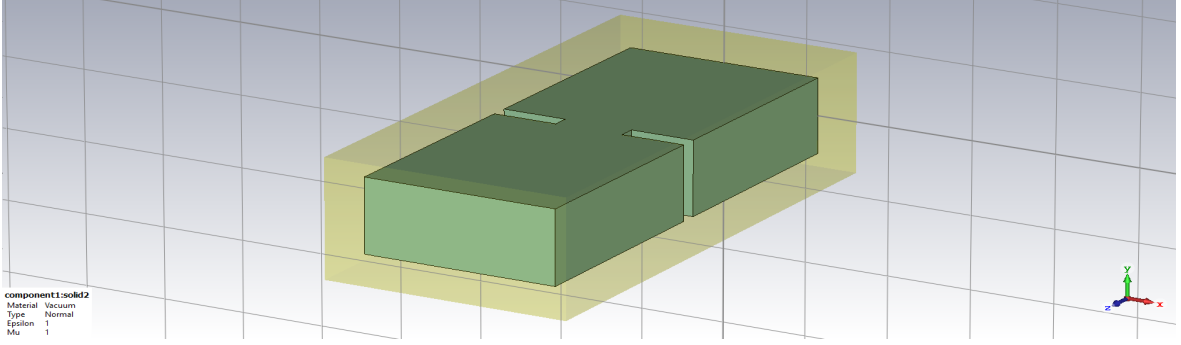
Figure 16: Two cavities connected by an inductive coupling

It is possible to calculate both frequencies by two different ways, the first one consists of a two cavities structure, like figure (16). In the even resonant mode, the sign of the E_y field of both cavities is the same, because that we call this mode as the phase mode. On the other hand, in the odd mode the E_y field of each cavity is the opposite, so we call this case as the contra phase mode. Figure (17a) and (17b) show the E_y field of the even and odd modes in a two cavities design coupled by an inductive irises. In this case we get $f_e = 8.298$ GHz and $f_o = 8.530$ GHz. As we can observe the even resonant mode appears before the odd mode, obtaining a negative value of the intra cavities coupling parameter k.
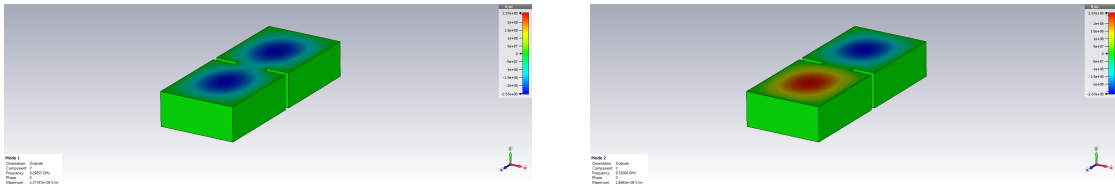

(a) E_y field of the even mode in a two cavities design

(b) E_y field of the odd mode in a two cavities design

Another way of calculating this pair of frequencies is making a vertical cut in the XY symmetry plane, obtaining a design as in the figure (18), in which there is only one cavity with an inductive iris. After that, we introduce a perfect electric condition (PMC) or a perfect magnetic condition (PEC) in the XY plane as boundary conditions. Analysing each case we get the even and odd frequency respectively. In this case, for a cavity with the same size than in the previous case, we obtain $f_o = 8.529$ GHz and $f_e = 8.298$. A quite similar result than the obtained before.

Parameter	physical dimensions (mm)
lfs	27
inductive iris ai	9.09
a	22.86
b	10.16
ti	1.7

Table 4: Physical system dimensions

The structure that we have used in this test has the parameters showed in table (4):
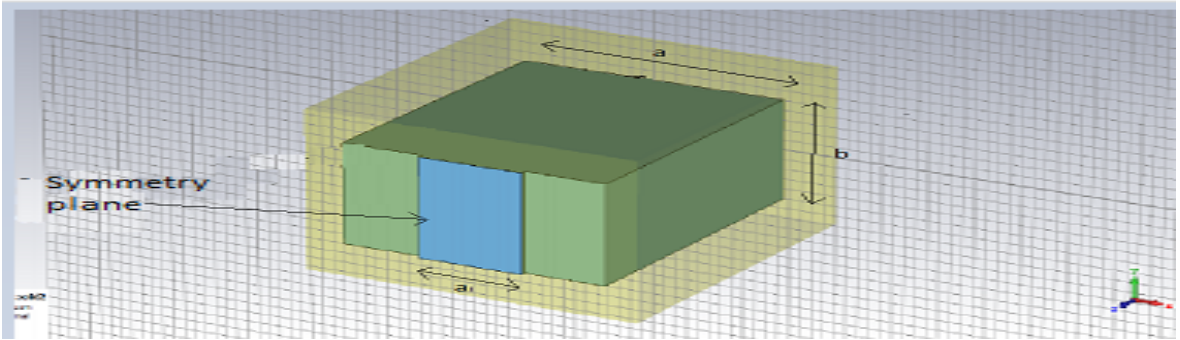
Figure 18: View of the structure when it is cut by the symmetry plane between the two coupled cavities

Now we are going to calculate a k value for our experiment. The k obtained following one of the two procedures can be observed in table (5). As we have described, the k factor is negative due to the inductive iris. This parameter depends directly on the iris width, the wider our inductive iris is, the greater k value we get. However, as it is explained in the degree thesis ([7]), if we extend the iris $width$, it will have a negative impact on the C factor, and consequently on the figure of merit F.O.M. Taking into account all the conditions and aspects mentioned, we have chosen a value of $|k| = 0.0377$, which is obtained with a cavity length $lc = 30.374mm$.

f_e	8.50984 GHz
f_o	8.19461 GHz
k	-0.0377

Table 5: Simulation results

We are ready for calculating the dimensions of the capacitive iris. Following the same procedure than in the inductive case, we obtain an iris height of 1 mm. Note

that the width of the inductive iris has a much higher value in comparison with the height of the capacitive iris. In both cases the resonator is formed by introducing an impedance change at the end of the resonators, so the energy is trapped in the middle. In the case of an inductive iris the change is very strong, since it changes the impedance from real to purely imaginary. That is why relatively wide irises are able to produce small couplings. In the case of a capacitive coupling, the impedance is always real. You can only change the value of the impedance from low real values to high real values. This is the maximum contrast that you can get, so to produce enough contrast in the impedance you need to produce very big skip. That is the reason the capacitive iris is so small.

We are going to simulate a five cavity filter with four capacitive irises we have calculated with the idea of emulating our first design in which all the irises was inductive. In this case, the phase mode is the fifth instead of the first, due to the influence of the capacitive couplings. In table (6) we are displaying the size of the structure whereas in figure (20) there is a view of the E-field of the fifth mode.

According with the theory we have seen in section 2, we have to force the eigenvector (1,1,1,1,1) for a matrix in which all the inter cavities parameters are positive and equal as follows

$$
\lambda \begin{pmatrix} 1 \\ 1 \\ 1 \\ 1 \\ 1 \end{pmatrix} = \Omega \begin{pmatrix} 1 \\ 1 \\ 1 \\ 1 \\ 1 \end{pmatrix} = \begin{pmatrix} \Omega_1^2 + K \\ K + \Omega_2^2 + K \\ K + \Omega_3^2 + K \\ K + \Omega_4^2 + K \\ K + \Omega_5^2 \end{pmatrix} \tag{23}
$$

We obtain the following relationships:

$$
\lambda = \Omega_1^2 + K = \Omega_5^2 + K \tag{24}
$$

$$
\lambda = \Omega_2^2 + 2 \cdot K = \Omega_3^2 + 2 \cdot K = \Omega_4^2 + 2 \cdot K \tag{25}
$$

To solve this system we have to enforce the inter-cavities coupling factor k and the eigenvalue λ. As we have described before, λ represents the frequency of the resonant mode associated with the eigenvector we have imposed. Once we have solved the equation system, we can show the eigenvectors obtained in equation (26).

$$
\begin{pmatrix} -0.1954 & -0.3717 & -0.5117 & -0.6015 & 0.4472 \\ 0.5117 & 0.6015 & 0.1954 & -0.3717 & 0.4472 \\ -0.6325 & 4.8295 \cdot 10^{-17} & 0.6325 & 2.2383 \cdot 10^{-17} & 0.4472 \\ 0.5117 & -0.6015 & 0.1954 & 0.3717 & 0.4472 \\ -0.1954 & 0.3717 & -0.5117 & 0.6015 & 0.4472 \end{pmatrix} \tag{26}
$$

As we can observe, the values of the eigenvector obtained for the fifth mode are equals and with the same sign. Theoretically, the fifth resonant mode is the one which couples to axions.

We are able to calculate the scattering parameter through the theoretical model. The scattering parameters of this structure are shown in figure (19), note that it is calculated without losses, so that when S_{11} tends to 0, or a very negative value in a logarithmic scale, then $S_{21} \simeq 1$, or 0 dB.

Parameter	value (mm)
a	22.86
b	10.16
Wc	0.5
ti	2
L1	26.68
L2	25
L3	25
L4	25
L5	26.68

Table 6: Physical dimensions of a five cavities filter with capacitive couplings.

In figure (19) and table (6) we show the E_y field of the five resonant cavities with capacitive irises and its physical dimensions respectively.

Observing figure (19), the fifth resonant mode is quite close to the fourth (poner MHZ), so we have the same problem than in the inductive irises cavity. In both structures, this proximity between modes will cause a huge instability to a tolerance geometric change in the structure, and it will be even more unstable when we increase the number of cavities.

As we can appreciate in figure (20), the highest field intensities are in the irises, with opposite sign with the cavities. That is caused because the capacitive irises are able to store energy. Due to that fact, the geometric factor C of this structure is very low independently of the value obtained theoretically in the eigenvalues and their respective eigenvectors. The problem with this design are mainly two, we did not find a solution in which the geometric factor C is high enough, and the fourth resonant mode is too near to the fifth mode, provoking the same instability issue than in the cavity system with inductive irises, making this design infeasible.
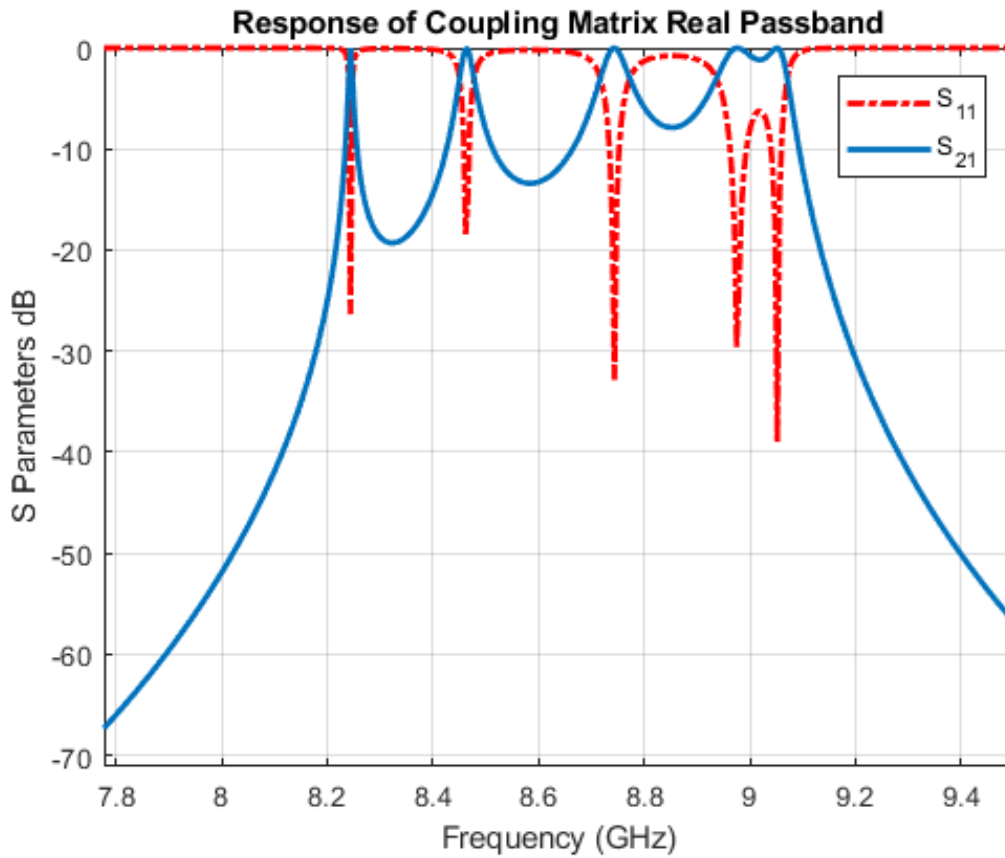
Figure 19: Scattering parameters of a five cavities system coupled by capacitive irises
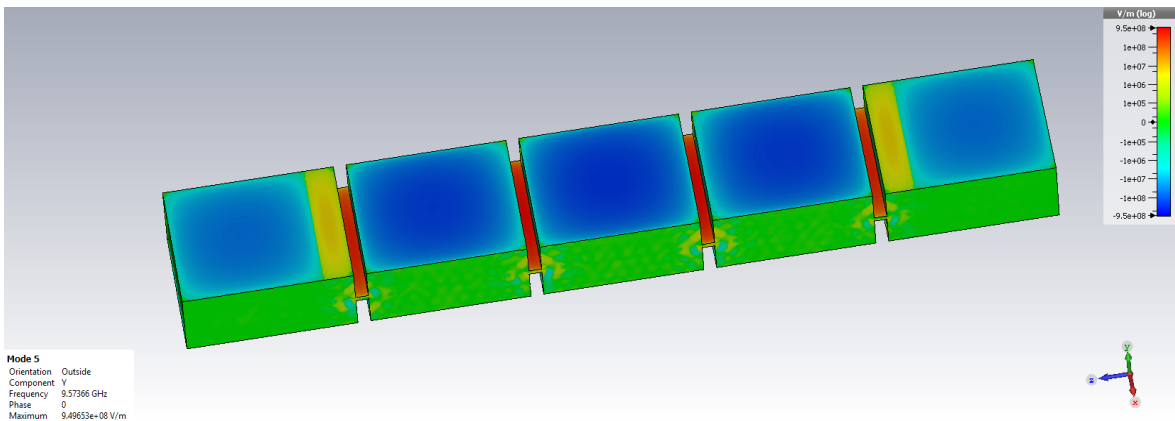
Figure 20: 5 cavities capacitive couplings, $\log(E_y\text{-field})$

Once we have seen the behaviour of a system in which its coupling are exclusively inductive or capacitive, the next step could be the design of a simple structure alternating both couplings. The idea consists of the design of a simple structure with alternating couplings, in which the phase mode that couples to axions will be located in a intermediate resonant mode. In this kind of structures, the number of cavities play an important role in the design. If we use an even amount of cavities N, the number

of couplings would we necessarily odd $N-1$ and we will have a symmetric structure. However the phase mode will not be located in the middle of our frequency bandwidth due to the fact that we have an even number of resonant modes. On the other side, if we design an odd number of cavities, we will have an asymmetric structure with a symmetric frequency spectrum. We have developed two structures with alternating couplings, with five and six cavities. The Scattering parameters of both systems are shown in figures (21a) and (21b) . As we have explained previously, in the odd case we have a symmetric frequency spectrum whereas for the even structure it is not. On the other hand. if we see pictures (22) and (23), we can observe that the six cavities system is symmetric. We are going to study the behaviour of the even structure. From this moment, we are going to call it the alternating couplings cavity.
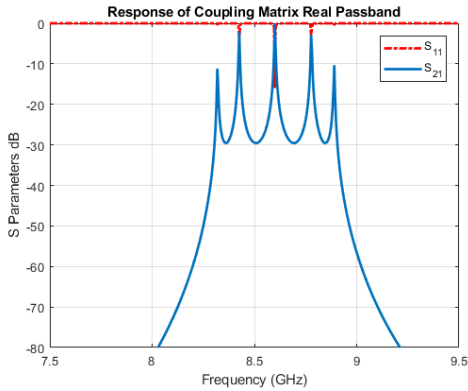
(a) S-param five cavities design
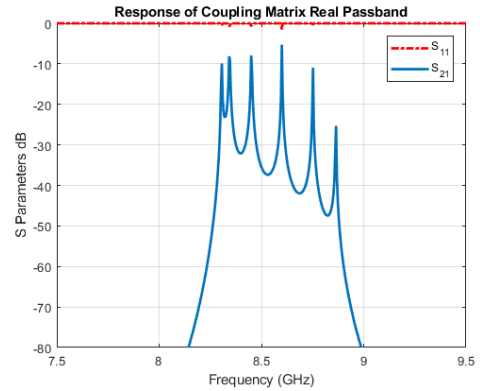
(b) S-param six cavities design

As we showed in the figure (23). In this design we have chosen 3 capacitive and 2 inductive couplers $(k-kk-kk)$ with the dimensions of the irises that we had obtained before. we have to increase the number of cavities to six in order to keep the geometry of the structure. As it is displayed in the picture (23, if we make a XY plane cut in the middle of the structure, we obtain two identical pieces. Whereas in our first inductive design the phase mode was the first and in the capacitive was the fifth, in this case, due to the alternation of coupling, the phase mode which couples to axions is the fourth. That is exactly what we were looking for. According to the theory seen in section 3, in the dispersion frequency curve the modes located in a intermediate frequency are more separated from the others.

Additionally, there is another aspect to be considered. Due to the geometry of the system, the are three additional resonant modes located at 6 GHz, one of them couples to axions. To understand why the system has this behaviour, we have to imagine that only the inductive irises are working as a couplers. Then we have a system formed by three long cavities joint by three inductive irises. Due to the fact that these "new cavities" are longer, the resonant modes are in a lower frequency range. Moreover, as we have only three new cavities, there are three resonant modes. we can conclude that the behaviour of this design is like a three sub-cavities system connected by inductive irises at 6 GHz and like a six sub-cavities system with alternated couplings at 8GHz.
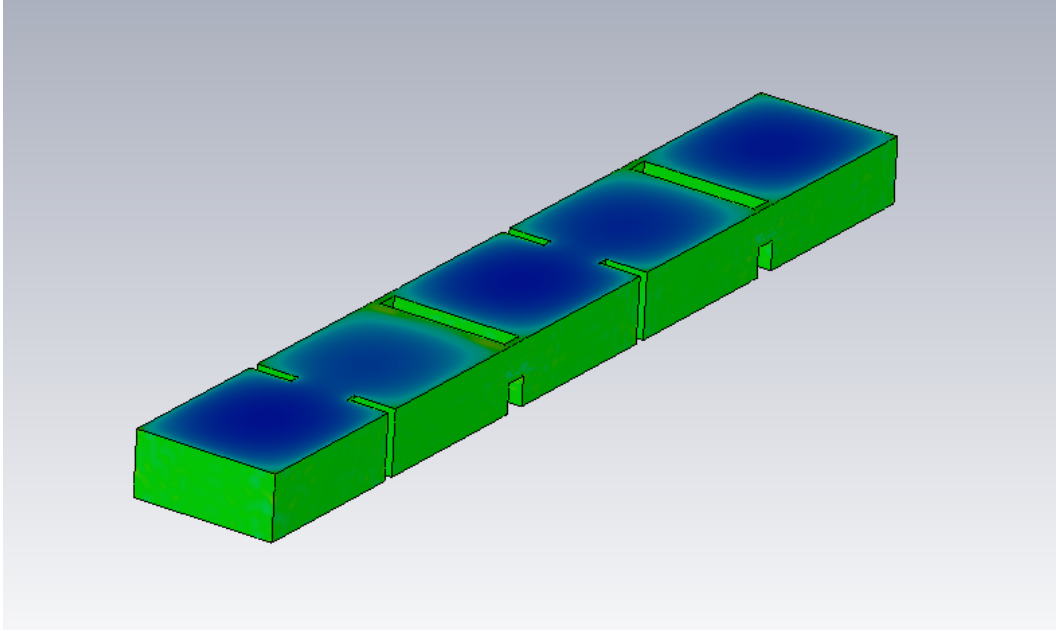
Figure 22: 5 cavities alternating couplings, $\log(E_y$-field)
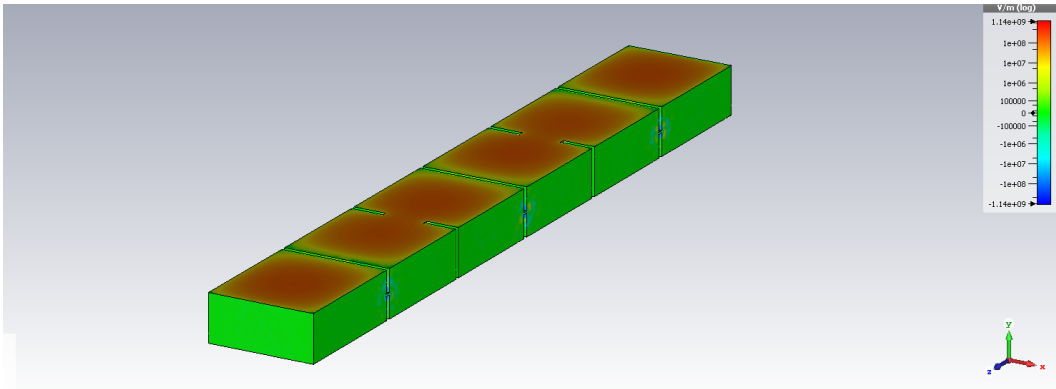
Figure 23: 6 cavities alternating couplings, $\log(E_y$-field)

The most important application for our experiment consists of using both modes for looking axions, increasing the frequency range by two.

Now we are going to show the E_y field for each resonant mode when the system is behaving as a six cavities filter (Figure 27), and as a three cavities filter (Figure 24). As we have explained above, we have two phase modes, modes 1 and 4 when the system works as a three or six cavities filter respectively.

Because of some manufacture problems with the design, we cannot fabricate the structure as we had designed. We have found a solution modifying the capacitive irises to a quasi-capacitive iris. Due to that change in the capacitive irises, there is less electric field stored inside them, then the electric field with opposite sign has decreased, so we
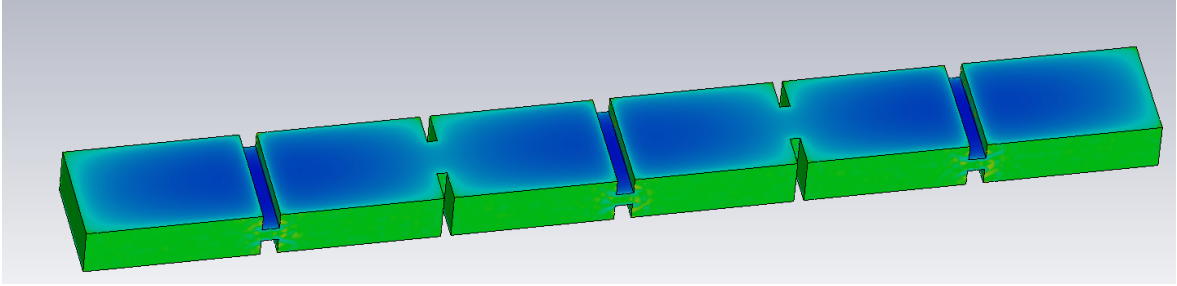
Figure 24: Six cavities design when it is behaving as a three cavities system
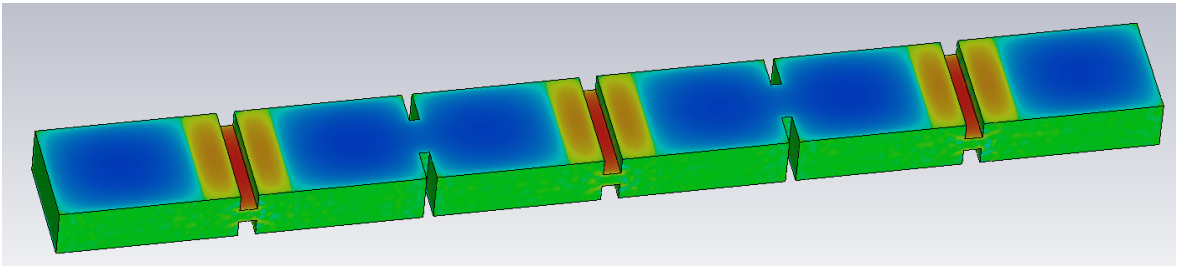
Figure 25: Six cavities design when it is behaving as a six cavities system

obtain a better C factor. The inductive irises has not been altered. the dimensions of this design are showed in figure (26). The probes have been introduced in the system in order to obtain the scattering parameters.
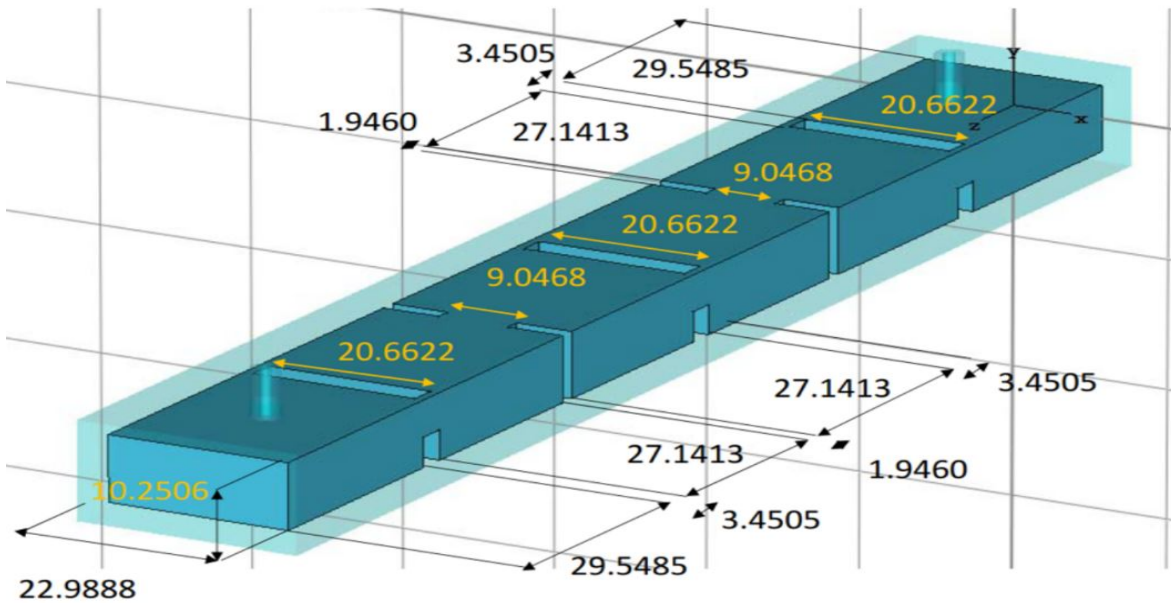
Figure 26: Six cavities design with inductive and quasi-capacitive coupling

In figure (27) we show the electric field of each resonant mode. We can observe that the only resonant mode in which the electric field is in phase for all the cavities is the fourth one.

(a) mode 1

(b) mode 2

(c) mode 3

(d) mode 4

(e) mode 5

(f) mode 6
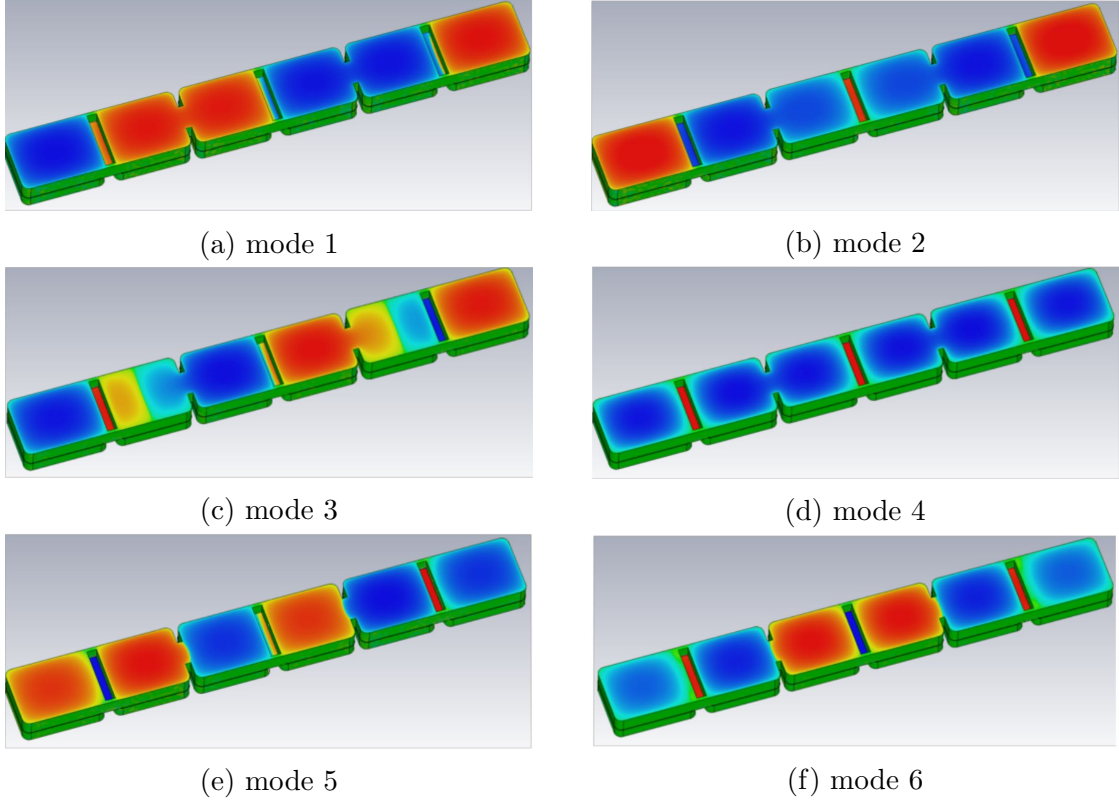
Figure 27: Schematic of E_y field for each mode of the six cavities design

In table (7) we show a comparison between our first 5 cavities design (Design 1), the new design with capacitive irises (Design 2) and the structure with quasi-capacitive irises (design 3) when it is behaving as a six cavity structure:

| Parameter	Design 1	Design 2	Design 3
C^2	0.65	0.512335	0.618833
Q	40386	28033.5	41330.5
Volume	$3.02 10^{-5}$	$3.58596 10^{-5}$	$3.9974 10^{-5}$
F.O.M.	$1.56 \ 10^{-5}$	$2.48372 \ 10^{-6}$	$2.52914 \ 10^{-5}$
Mode 1 frequency	8.428 GHz	8.50706 GHz	8.18762
Mode 2 frequency	8.454 GHz	8.57515 GHz	8.21562
Mode 3 frequency	8.528 GHz	8.70721 GHz	8.29073
Mode 4 frequency	8.625 GHz	8.9441 GHz	8.38477
Mode 5 frequency	8.710 GHz	9.09981 GHz	8.51107
Mode 6 frequency	-	9.24052 GHz	8.59725

Table 7: Results of 5 cavities simulation

Note: All the parameters (apart from frequencies) have been calculated with the E-field of the mode 1 in the first design and with the mode 4 in the other two cases.

From the data obtained in the table (7), we can appreciate that, although the first design gets a better value of the geometric factor C, in the third case we obtain a higher frequency separation between our phase mode and the rest (26 MHz vs 126.3 MHz). Moreover, in this last design, we have increased the quality factor value and the volume of the structure, getting also an increment in the F.O.M. The advantages of this design are mainly three, a more stable design against tolerance geometric changes in the structure, a higher F.O.M value, and an increment in the frequency separation between resonant modes.

Now we can try with a bigger system, like 30 cavities. In this design, the phase mode will be the 16th as we can see in the figure 28. Due to the increment in the number of sub-cavities, its dimension has undergone several changes from the 6 cavities system.
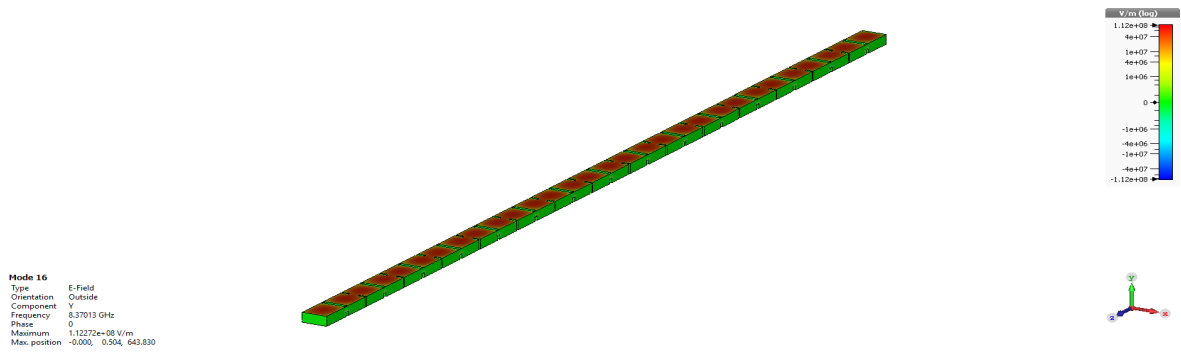

Figure 28: 30 cavities alternating couplings, $\log(E_y$-field)

Parameter	dimensions
C^2	0.625718
Q	40399
Volume	$1.1963 10^{-4}$
F.O.M.	$6.1564\ 10^{-4}$
Mode 14 frequency	8.35573 GHz
Mode 15 frequency	8.37013 GHz
Mode 16 frequency	8.40635 GHz

Table 8: Results of 30 cavities simulations

In this case, from the data of table (8) we get a frequency separation of 36.2 MHz, a higher value than in the original design of 5 cavities in which the phase mode was the first (36.2 MHz vs 26 MHz). As far as the frequency is concerned, this 30 cavities system seems to be more stable than a 5 inductive cavities. As we have obtained in equation 27, the total length of this structure is 0.924m. Although it is enough space to introduce an extra couple of cavities in the experiment room, we think that it is better to leave some additional free space. This system has been manufactured and it is going to be measured at CERN.

$$L = 2 \cdot lfs + 28 \cdot lc + 14 \cdot ti + 15 \cdot tc + 2 \cdot thick = 0.924(m) \qquad (27)$$

As we have a huge amount of cavities, we can show the frequency dispersion curve of the different resonant modes. We can appreciate that, as well as we could see in the periodic boundary condition section, the modes which are located in the middle are more separated of the rest of resonant modes. We can say that the theory seen in the periodic boundary conditions section agrees with the results we have obtained here.
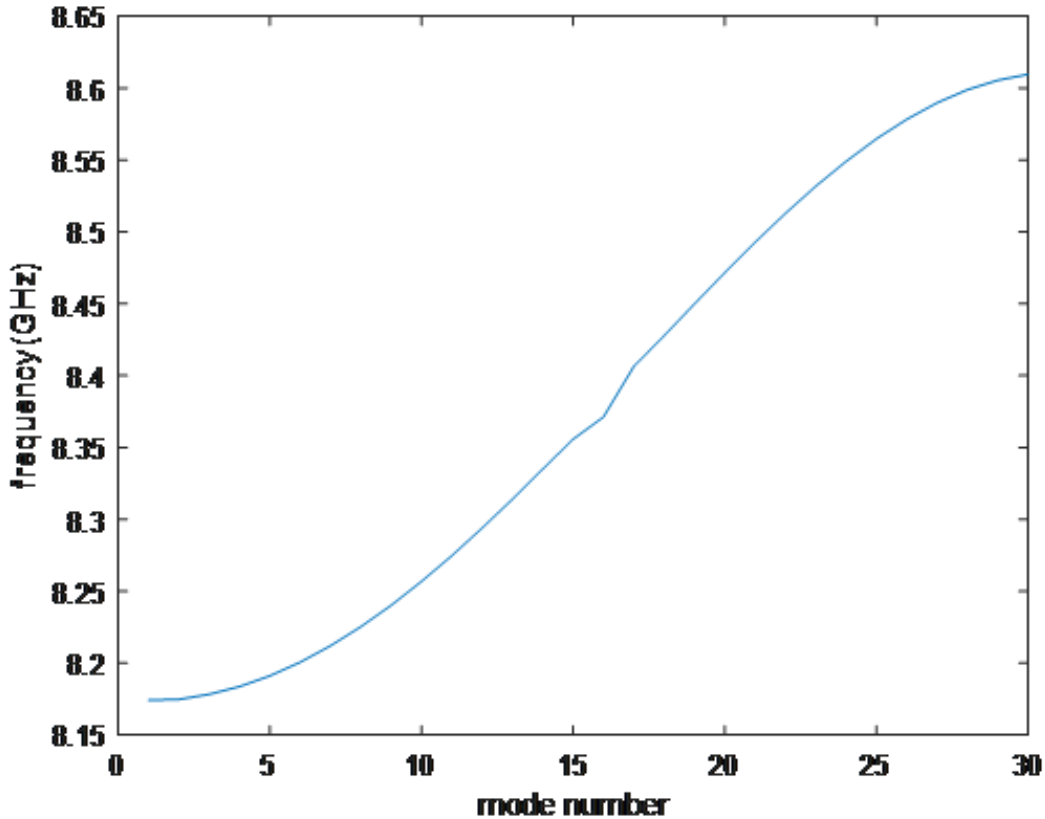
Figure 29: Frequency dispersion curve for a 30 cavities design

4.2   Ports coupling

Once we have described our design: a six cavity system with the capacitive and inductive irises, the next step consists of finding the critical coupling point in which we get the best value of quality factor Q, introducing probes in the first and last cavities. According to the theory seen in section 1, for our application the higher Q_l value happens when the unloaded and loaded quality factors are equal. In this section, we are going to explain procedure to find the critical coupling point and the relationship between it and others parameters such as the quality factor Q.

As we have explained previously, our system is critically coupled to a feedline when $\sum Q_e$ is equal to Q_u. The Q_u is given by the material properties such us the conductivity, it can be modified by changing the temperature. The Q_e is modified by the geometry of the global system. Once it is manufactured, we cannot change the dimensions of the cavity structure, so the only way of modifying this factor is through the feedline geometry. We are going to use a coaxial cable, so in order to change the geometry, we will alter the depth of the probes (inner coaxial conductor) inside the cavity.

4.2.1   Simulations

In this part, we will show the procedure we have carried out to obtain the critical point of the fourth mode using the scattering parameters. Finally we display all the results obtained in the simulations with different materials and varying the temperature.

Before starting we should explain that, although the structure is designed with two ports, we are going to use only one port so the second port will be weakly coupled. Then, the external quality factor of the second port will be so high that it does not affect to the global Q_L. Additionally, as it is explained in [7], the behaviour of this structure is identical to a system with only one port.

Due to the fact that we do not have a formula or mechanism for calculating which is the best geometry in which the critical coupling point is located, we carry out a parametric sweep; it allows us to find the critical point by a final fine tuning. As an example we are going to find the critical coupling for the fourth resonant mode of the alternated couplings cavity at a cryogenic environment (temperature of 4K), at this temperature, the cooper has a theoretical conductivity of $2.008 \cdot 10^9 \frac{S}{m}$. In figure (30) we can appreciate a parametric sweep of the probe length with steps of 0.4mm. Looking this sweep, we can extract some details:

- In figure (30a), The probe is not enough introduced in the cavity, which means that all modes are weakly coupled.

- In figure (30c), modes 1 and 2 are strongly coupled, it occurs because of the frequency split between both modes is quite small (under 0.2 GHz). Moreover, the fifth mode is strongly coupled when lhot = 0.2mm, as it is shown in figure (30d). According to what we explained in theory, the critical coupling point of each mode depends on its frequency, as we are looking that the fourth mode will be strongly coupled, we should do a fine tuning of lhot from -0.2mm to 0.2mm.

- Finally, in figure (30f) the six modes are overcoupled.

Now, with a fine tuning we obtain the critical coupling point for the fourth mode, which is located with a probe length of 0.02 mm inside the cavity, as we can observe in figure (31). In this case, whereas all the modes situated before the fourth are overcoupled, the fourth mode is strongly coupled, and the last modes are undercoupled.
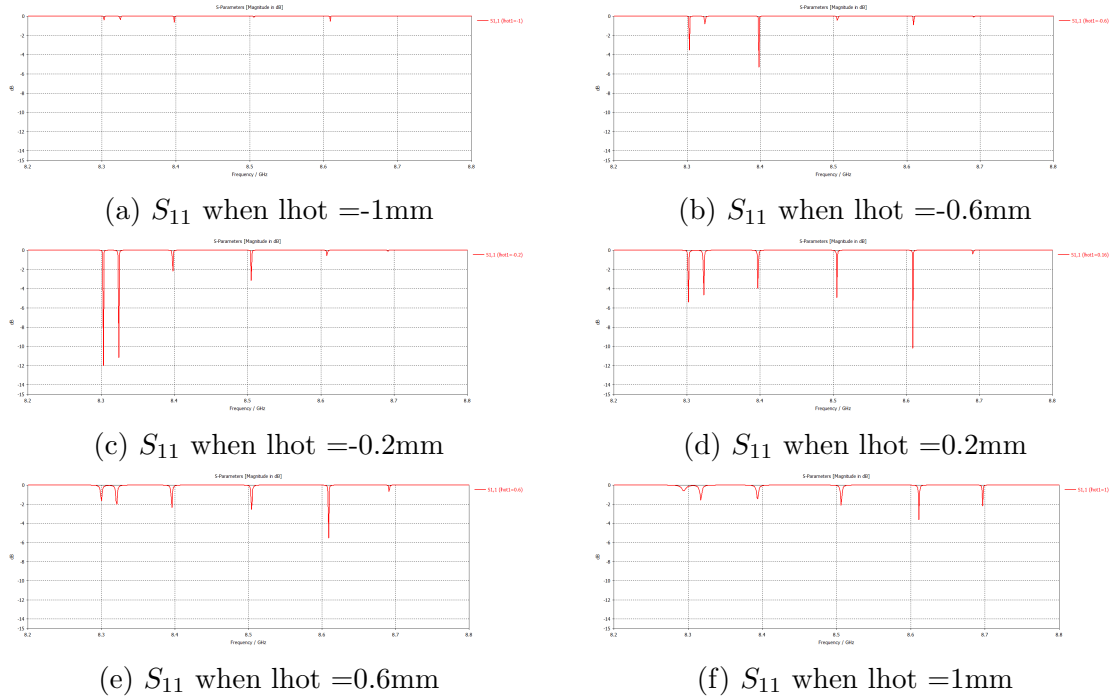
(a) S_{11} when lhot =-1mm

(b) S_{11} when lhot =-0.6mm

(c) S_{11} when lhot =-0.2mm

(d) S_{11} when lhot =0.2mm

(e) S_{11} when lhot =0.6mm

(f) S_{11} when lhot =1mm

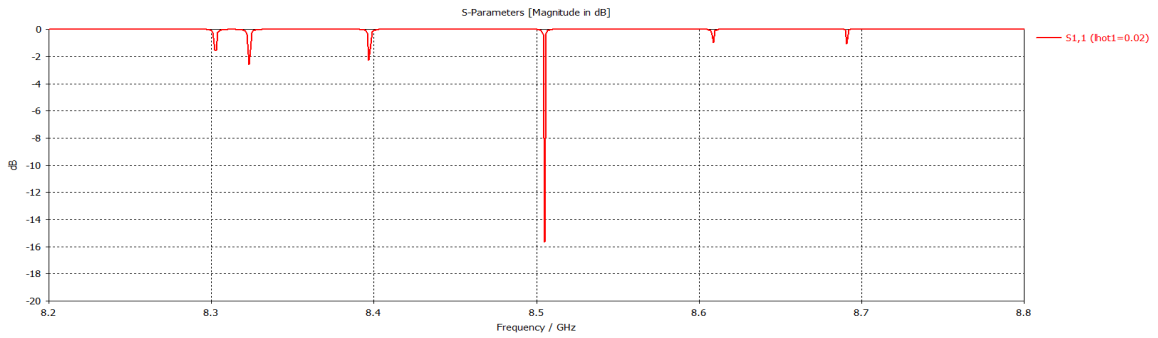Figure 30: Evolve of S_{11} parameter with different probes length

Figure 31: S_{11} parameter with lhot=0.02 mm and at cryogenic temperature

We can appreciate the evolution of the fourth mode adaptation from the variation of the probe length lhot. It is displayed in figure (32)

Although the adaptation of the fourth mode seems a bit unstable due to the high conductivity, we are able to find the critical coupling point at 0.02 mm. Figure (32) allows us to understand the behaviour of the coupling, from 0.02 to 0.2 mm the resonant mode is strongly coupled. The points before and after this interval are undercoupled and overcoupled respectively.
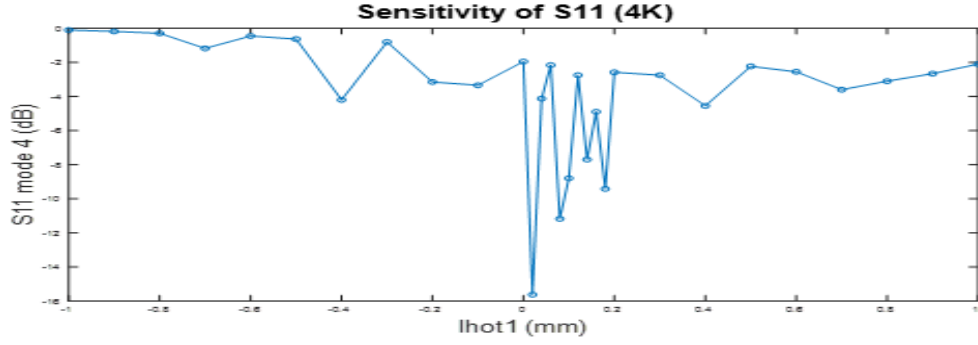
33

Figure 32: Adaptation of the fourth mode in dB scale

Following the same procedure we did at cryogenic temperature, we can find at room temperature the critical point, which is located when the probe is introduced at - mm inside the cavity. We could appreciate the S_{11} parameter in figure 32 and the evolution of the fourth resonant mode sensibility varying the length of the probe.

Finding the critical coupling point at room temperature did not represent a challenge. At this environment, the conductivity is not high, so the simulations run quite fast and the critical point is very stable. Nevertheless, when we are at cryogenic temperature the situation changes. The optimum coupling becomes more difficult to be found and the simulation needs more time until finishing.

4.3   Pros and cons of alternated couplings cavity

The alternating irises system presents several advantages such as the stability and the frequency difference between the mode which couples to axions and the rest. Several tolerances studies have been realised. We did a montecarlo analysis where the input parameters are the physical dimmensions and the output parameter is the C factor. As it is shown in figure (33), we can appreciate that the system is very stable. On the other hand, in order to obtain a suitable simulation, we need a huge mesh in the Software. However, if the mesh is too high, the software cannot find a solution and it stop immediately, giving us a wrong result. Additionally, the manufacture of a system of such characteristic is a complete challenge.
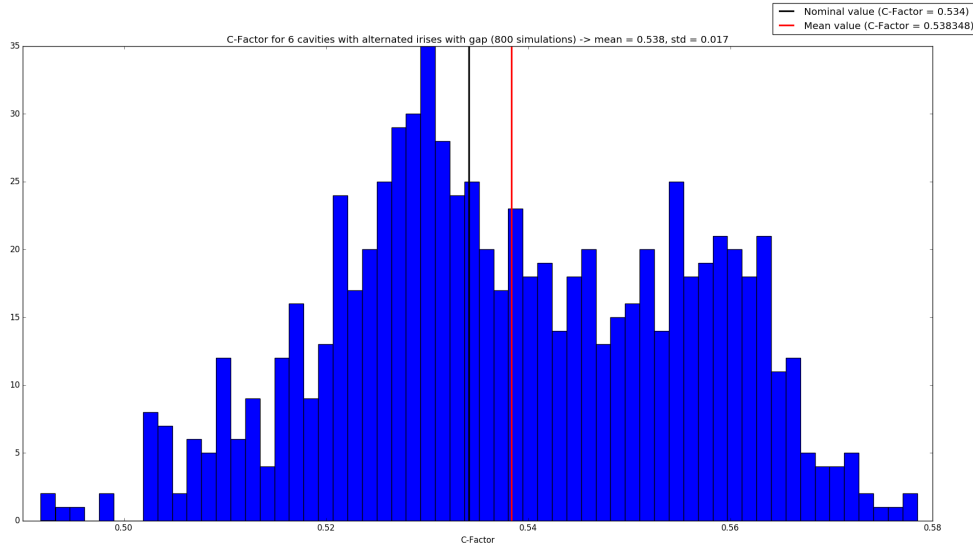
Figure 33: Frequency dispersion curve for a 30 cavities design

5 Tunable cavity

Once he have designed and tested different systems, the next step consists in doing a tunable cavity system. In this section we are going to describe the technology we have used as well as how is the behaviour of the inductive and alternated coupling cavities in simulations.

5.1 Theoretical explanation

In this part of the project we are designing a mechanical tunable cavity. The idea consists of dividing the cavity in two identical halves. Although there are infinite planes for doing the cut, there is only one in which the electric field that scape from the structure would be minimum. For instance, in figure (34) we can observe that the minimum H_{tan} is located at the symmetry plane ZY when the x axis is equal to zero.

doing a cut in the ZY plane the structure will be as shown in figure 35a.

5.2 Inductive irises cavity

In this part we are going to create a tunable inductive cavity by introducing a vacuum brick in the middle of the system as in figure (35a) and (35b). The idea consists of the separation of the inductive cavity shown in figure 6 in two identical halves by doing a vertical cut. Afterwards, increasing the separation between both parts, the volume will increase so that the frequency of the resonant modes will be reduced as expected.

The evolution of the first resonant mode from the vertical cut separation is displayed in figure (36).
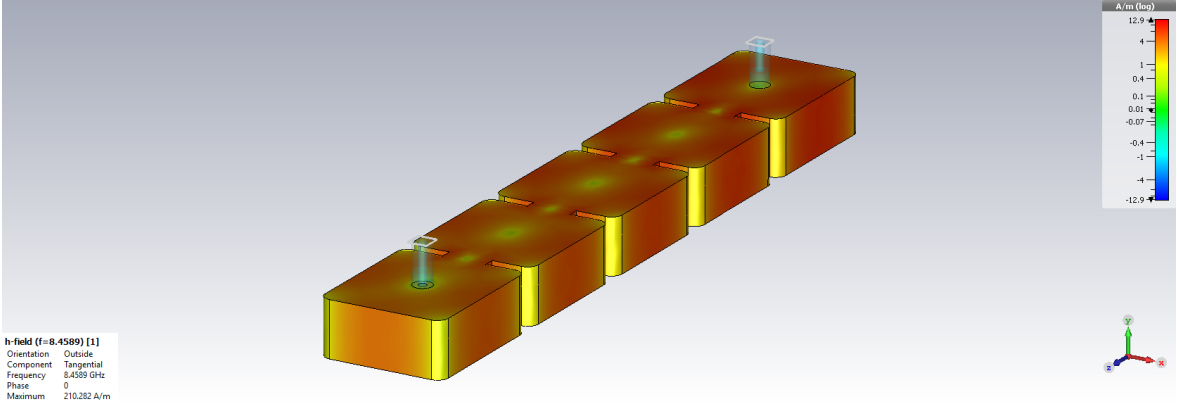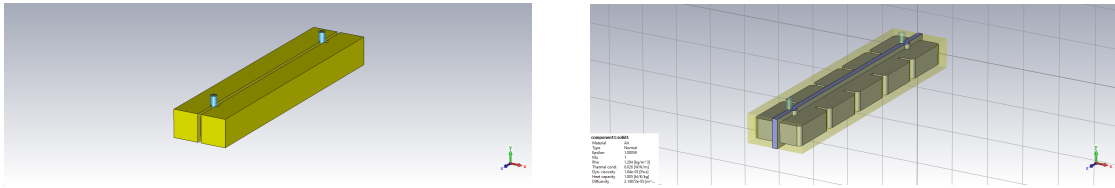
35

Figure 34: H_{tan} of a six sub-cavities structure

(a) CST design of six cavities with inductive irises and vertical cut

(b) CST design of six cavities with inductive irises and vertical cut
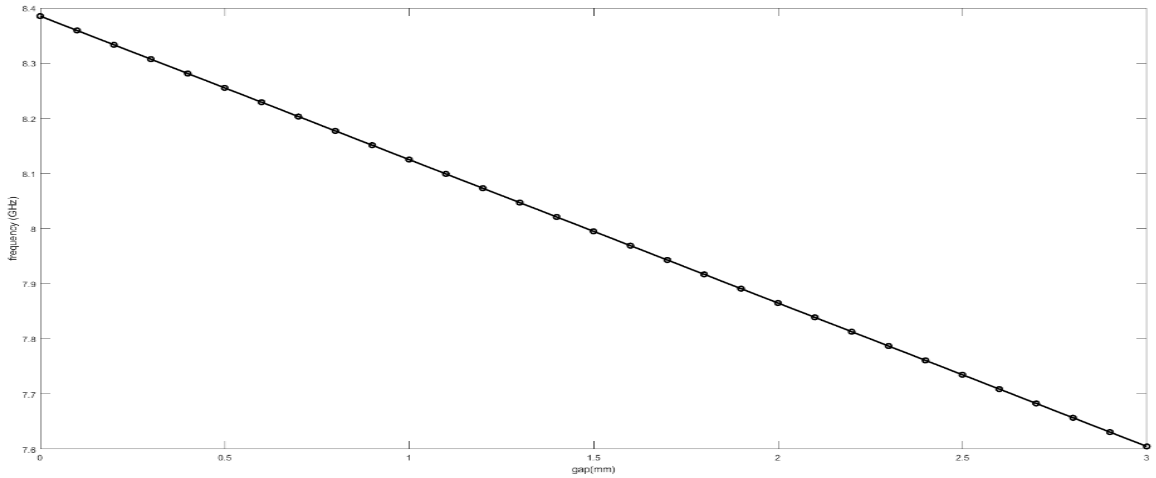

Figure 36: Mode 1 frequency increasing the width of the vacuum brick

Due to the vertical cut, it seems relevant to see the radiated power from the gap width. In order to calculate this parameter, we have eliminated the material losses changing copper to PEC, so that the power which is not transmitted nor reflected must be radiated. We are able to obtain both powers, transmitted and reflected, through the Scattering parameters, then we can calculate the radiated power P_r using the equation (28), where S_{11} and S_{21} are the reflected and transmitted power respectively.

$$P_r = 1 - |S_{11}|^2 - |S_{21}|^2 \qquad (28)$$

In equation (28) we are calculating the radiated power from the power available in the generator, another interesting idea could be calculate the radiated power from the port one instead from the generator as follows:

$$\frac{P_r}{P_{L1}} = 1 - \frac{|S_{21}|^2}{1 - |S_{11}|^2} \tag{29}$$

The most interesting part of this relation is that we are able to see the radiated power without taking into account reflections, providing us a general idea about how much power is transmitted or radiated. Using equation 28, we calculate the radiated power versus the gap width. In figure (37), we observe that the radiated losses are basically zero until the gap is approximately 2.5 mm wide, which corresponds with 10 dB loss. Once the gap is wider than 3.5 mm the resonance vanishes and consequently the transmitted power decreases dramatically. The radiated power has a maximum at 4 mm before the resonance disappear. In the light of these results, it seems that the gap width must be below 3mm, after this point, we can consider the radiated power is practically equal to the power available in port 1, which means that most part of this power is radiated.
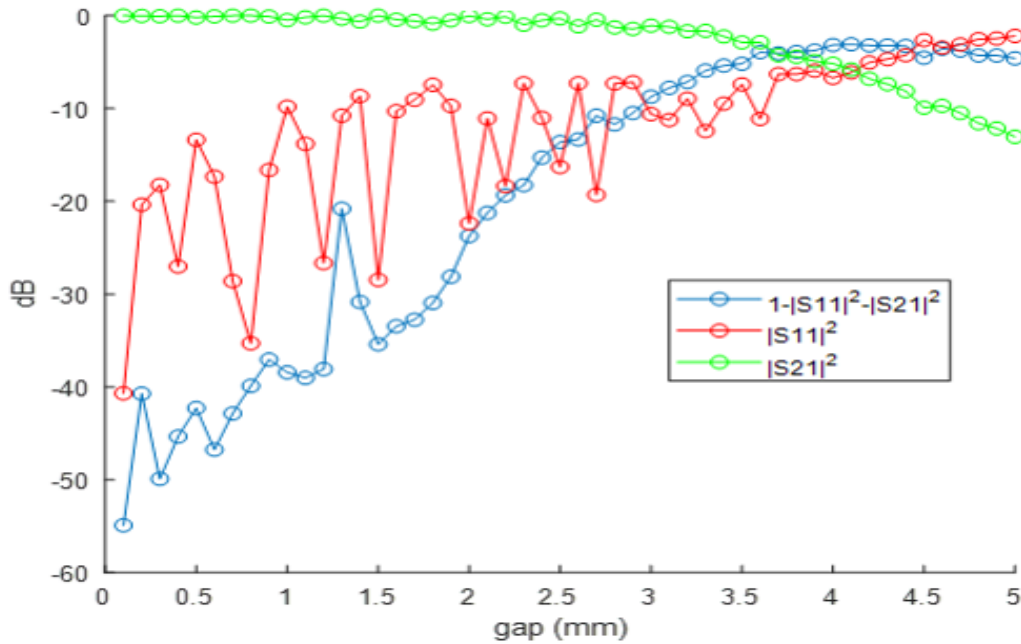

Figure 37: Radiated (blue), reflected (red) and transmitted power (green) vs gap width

It could be interesting to see how the probe location affects to the radiated power. In the previous simulation we place both probes in the cavity centre. Now we are going to situate both probes in the middle of one of the half cavity as it is shown in figure (38).
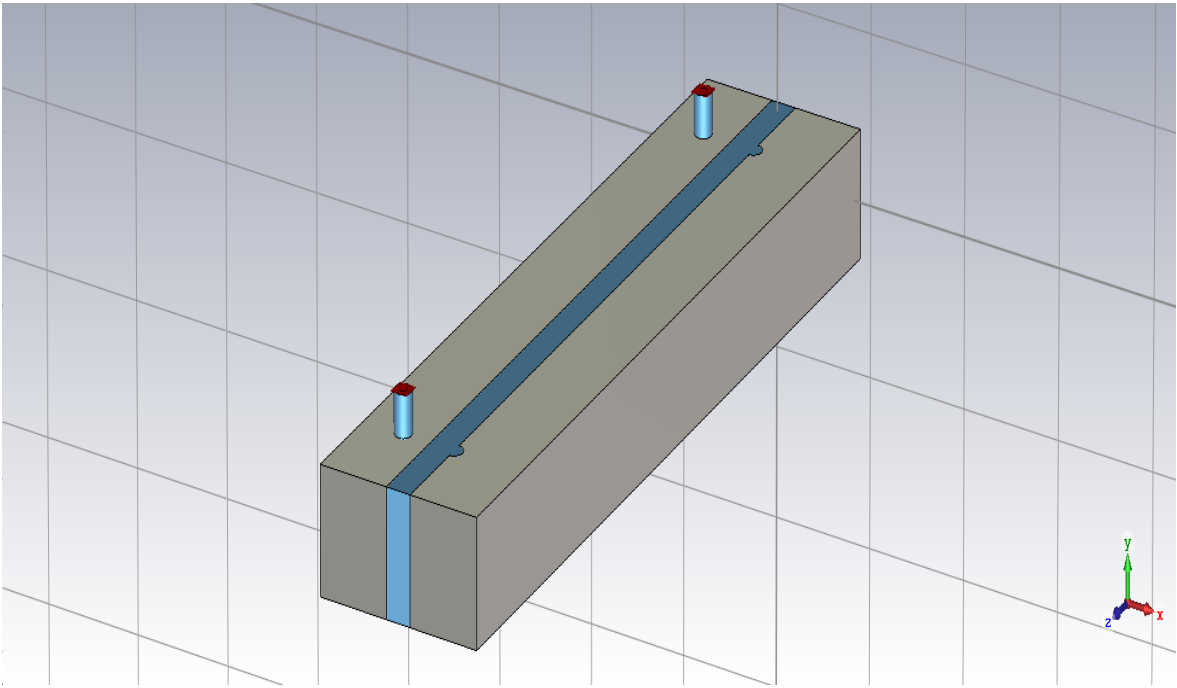
Figure 38: Radiated (blue), reflected (red) and transmitted power (green) vs gap width

The procedure for getting the radiated power is exactly the same than in the previous case. According to the equation (28), the results are displayed in figure (39)
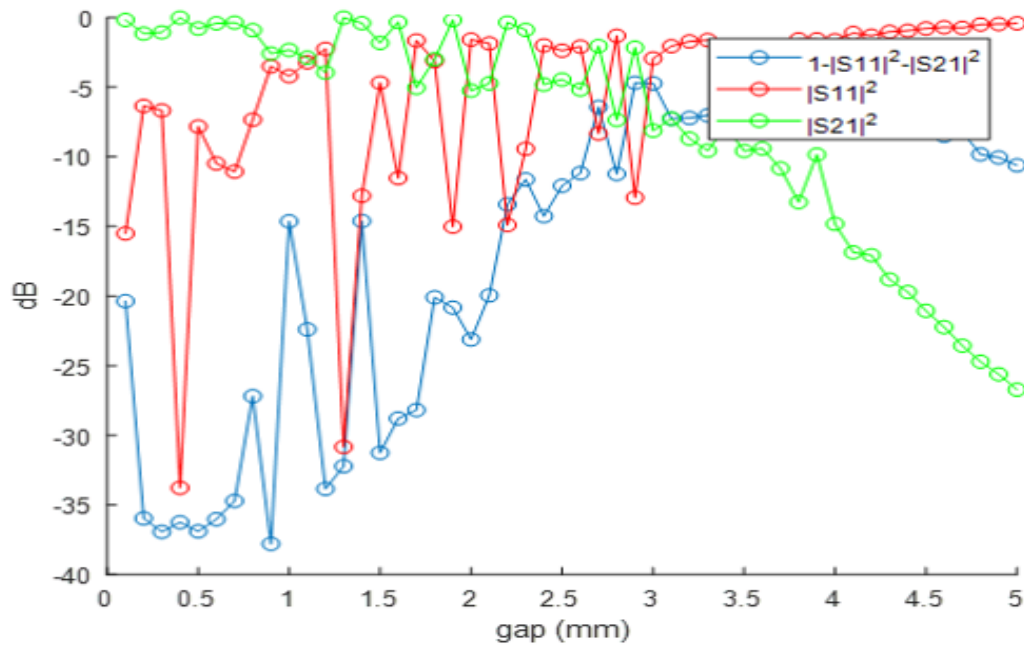

Figure 39: Radiated (blue), reflected (red) and transmitted power (green) vs gap width

Another interesting parameter to be monitored is the inter-cavities coupling k.

Although the equation to obtain this factor was described previously (see equation **??**), due to the gap the design to calculate both frequencies, even and odd, has undergone several changes. As we can appreciate in figure (40), we introduce the gap in the middle of the structure. Additionally there are two extra cavities in order to feed the two cavities design with the gap. The inductive irises among the external and internal cavities must be narrow so that in the structure response should appear only two resonances as we show in picture 41. The first resonance corresponds with the even frequency whereas the second one represent the odd frequency. The behaviour of this parameter is shown in figure (42) for a gap range from 0 to 3mm, which is the region of interest.
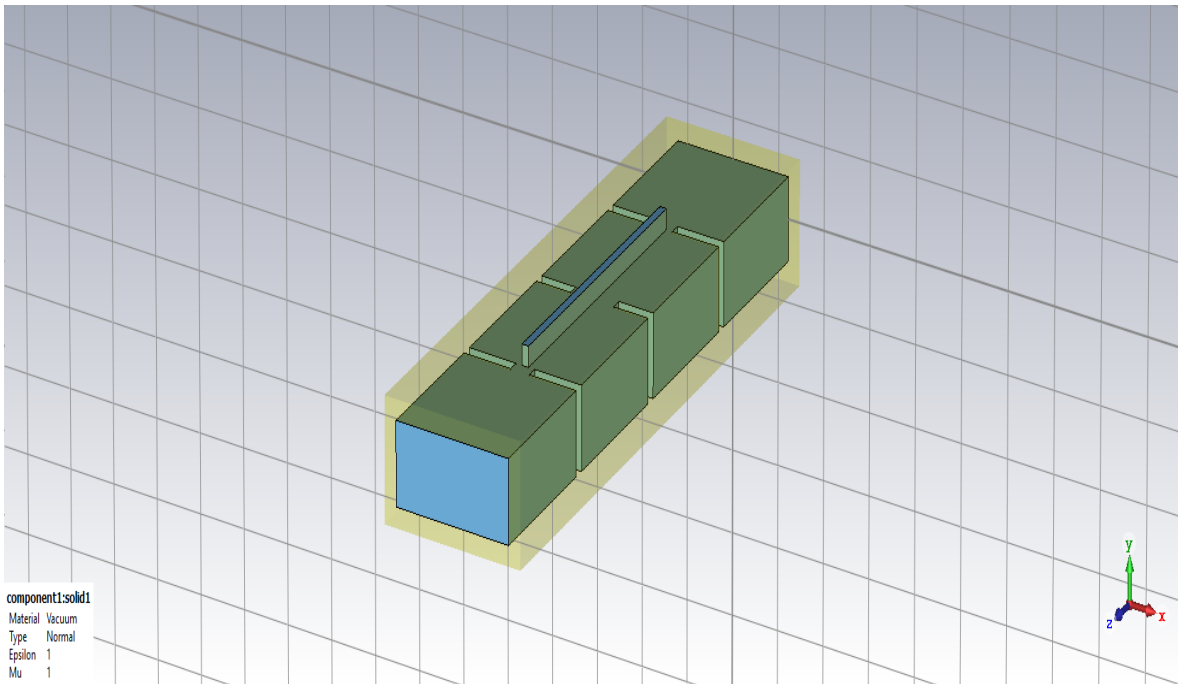

Figure 40: Design to obtain the inter-cavities coupling k

Observing figure (42), we can appreciate a lineal behaviour of the inter-cavities factor. Moreover the difference between the biggest and the smallest values is practically 0.03, which means that, as far as k factor is concerned, the coupling to the axion will be practically stable.

Once we have seen that the previous parameter are quite stable, the next step consists in calculating two of the most relevant parameters of this section, which are the axion coupling C and the quality factor of the system. As we saw in the first chapter, both parameters play an important role in the axion figure of merit F.O.M.
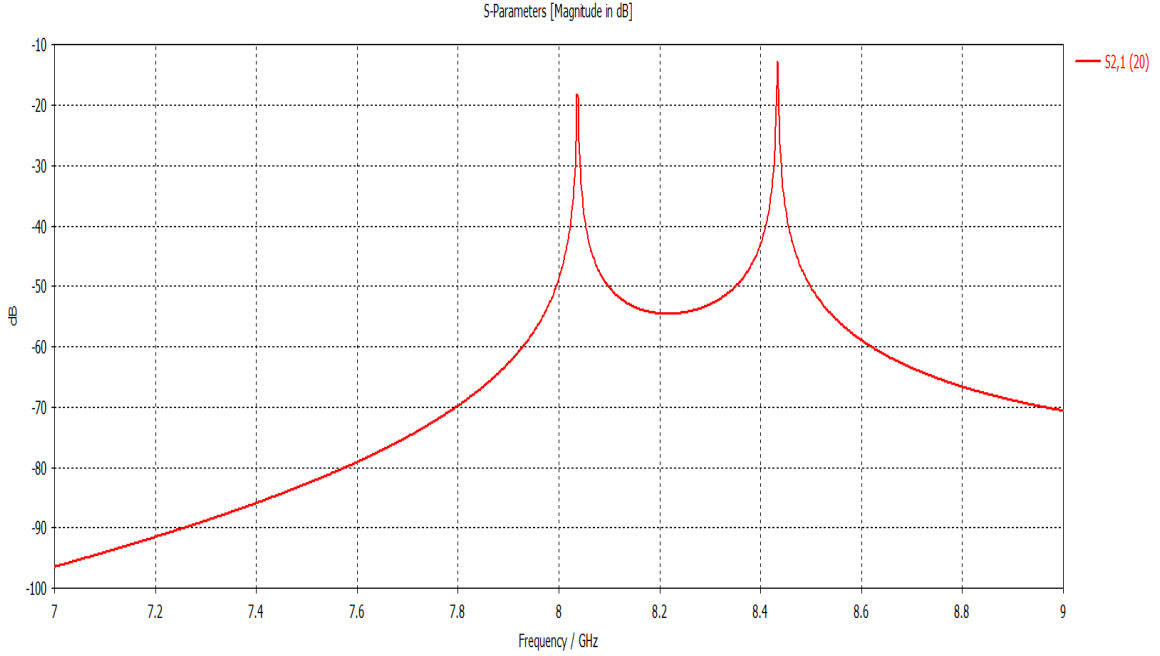
Figure 41: S21 parameter used to obtain the inter-cavities coupling

Both parameters, C and Q factors, seem to be quite stable from a gap range to 2mm, which means that we can have a tunable system of 700 MHz without undergoing great changes. From this point, the C factor decreases linearly with the gap width.

Additionally, another relevant aspect to be taken into account is the structure misalignment. Principally, the system could be misaligned in two directions, vertical and horizontal, we are going to see the structure behaviour in both cases for two different gap lengths. First of all, we are going to calculate the radiated power from de power available in port 1 for a gap length of 1.5 mm. The vertical and horizontal misalignments have been simulated to 2 millimetres with steps of 0.2 mm. The result is displayed in figure (45)

From picture 45, we can obtain several conclusions, the vertical misalignment has a greater impact in the radiated power than the horizontal. We can appreciate that due to the fact that when the vertical misalignment is greater to 0.3 mm, the radiated power is practically equal to the power available in port 1, whereas it happens in the horizontal misalignment at 1.8 mm. Additionally, we can pay no heed to the radiated power caused by misalignment when it is lower than 0.2 millimetres in both cases, horizontal and vertical.

The next step consists in the calculation of the radiated power in the region of interests that we have described above, but for another gap length, we now study 3.5 mm, which is the limit value that we have chosen previously.
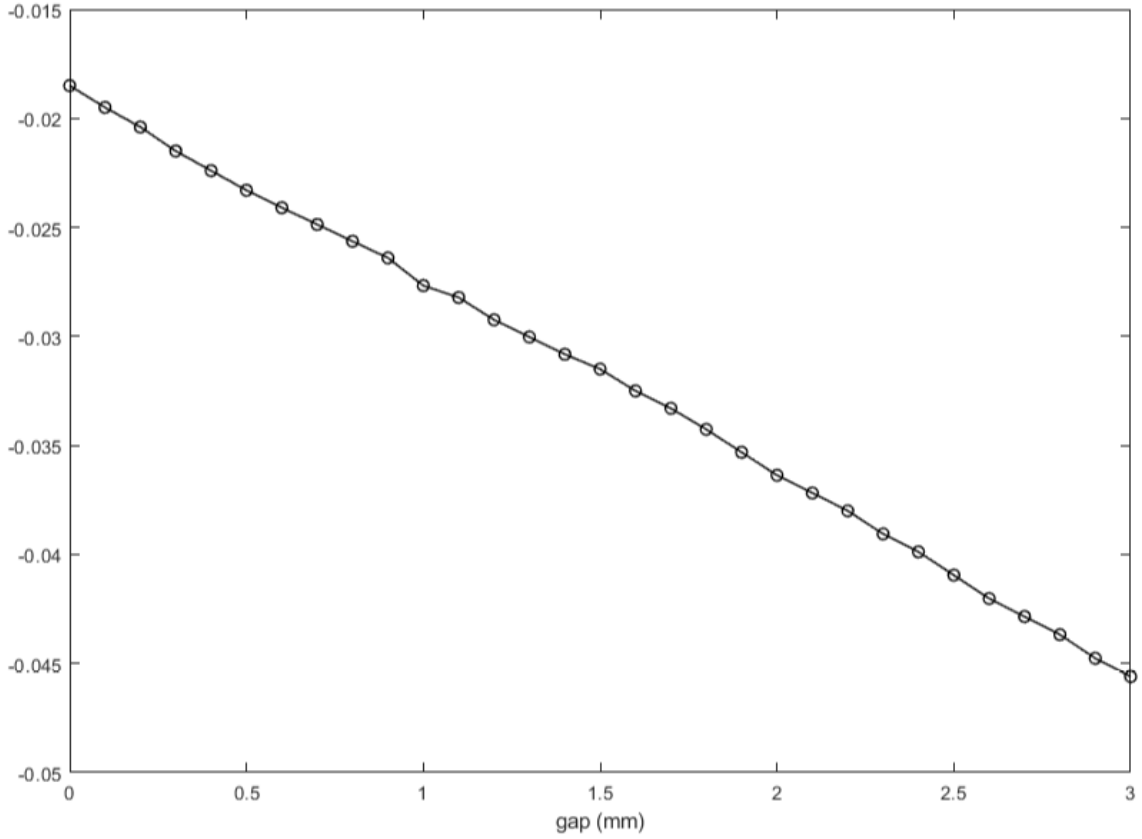
Figure 42: Variation of inter-cavities factor

In figure 46 we can appreciate that, as well as in (45), the vertical misalignment increases the radiated power more than the horizontal. Moreover, we can appreciate that, in a logarithmic scale, the growth of the radiated power is lineal with the vertical misalignment.

Due to the importance in this project, additionally we are going to calculate the variation of Q_u and Q_l. The Q_l is going to be calculated as we have described previously. However, in the case of calculating the Q_u, we are not going to use the CST calculator. As we know from equation (??), this factor depends on the Q_e of both ports as well as on Q_u. We define both ports extremely weakly coupled, so that both Q_e and Q_e will be such a high value that Q_l will be practically equal to Q_u.

$$\frac{1}{Q_l} = \frac{1}{Q_e} + \frac{1}{Q_e} + \frac{1}{Q_u} = \frac{1}{Q_u} \tag{30}$$

This way of calculating the Q_u is faster than using the CST solver because this method does not require any kind of mathematical integration,

Finally we are going to calculate the distance from the first resonant mode to the next one as it is shown in figure 47.
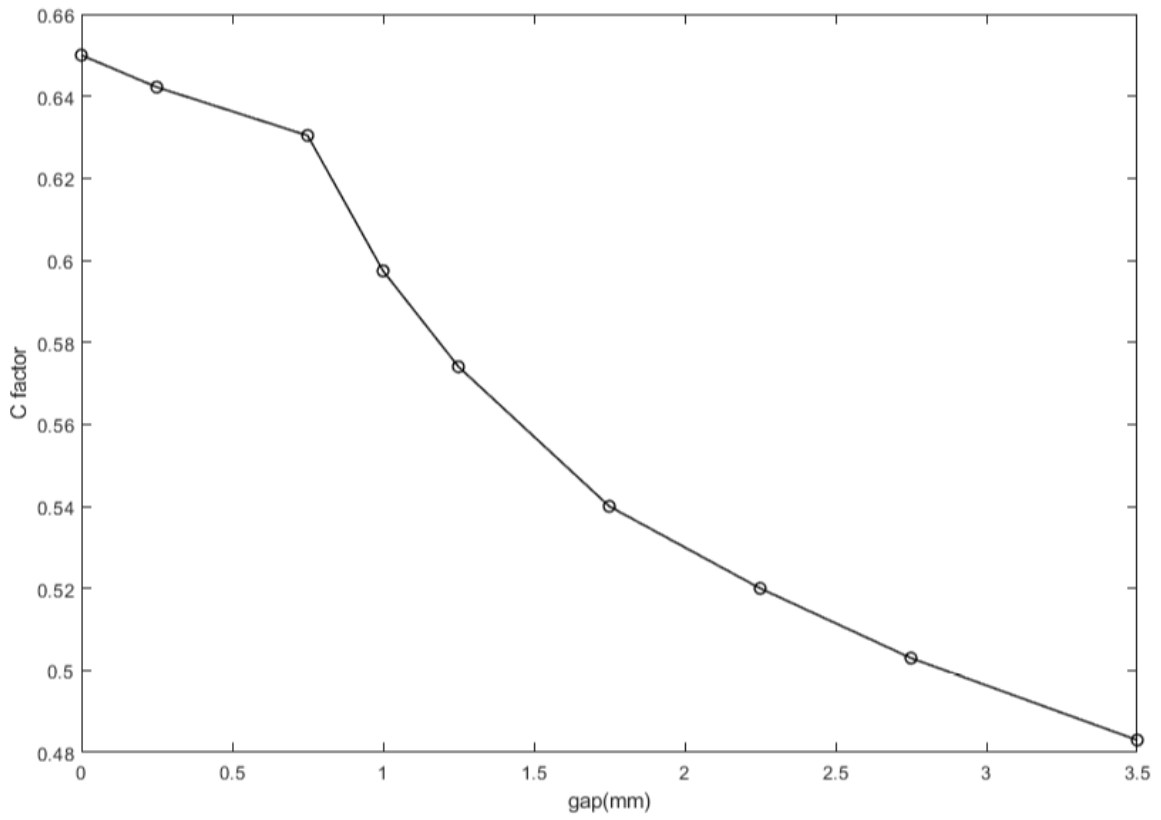
41

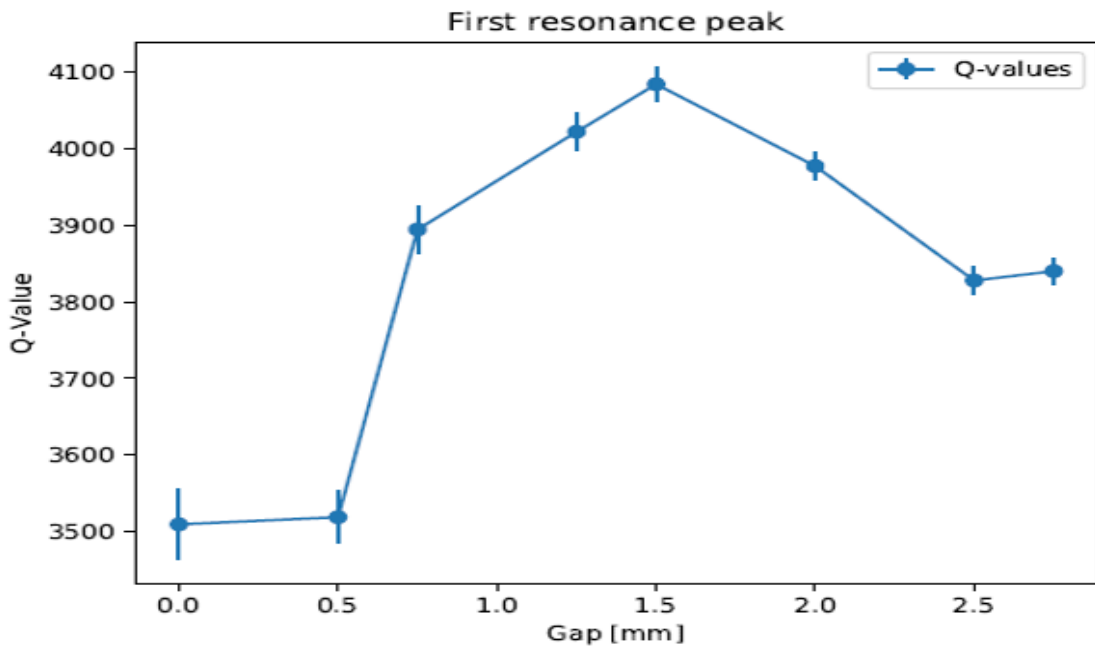Figure 43: Variation of C factor
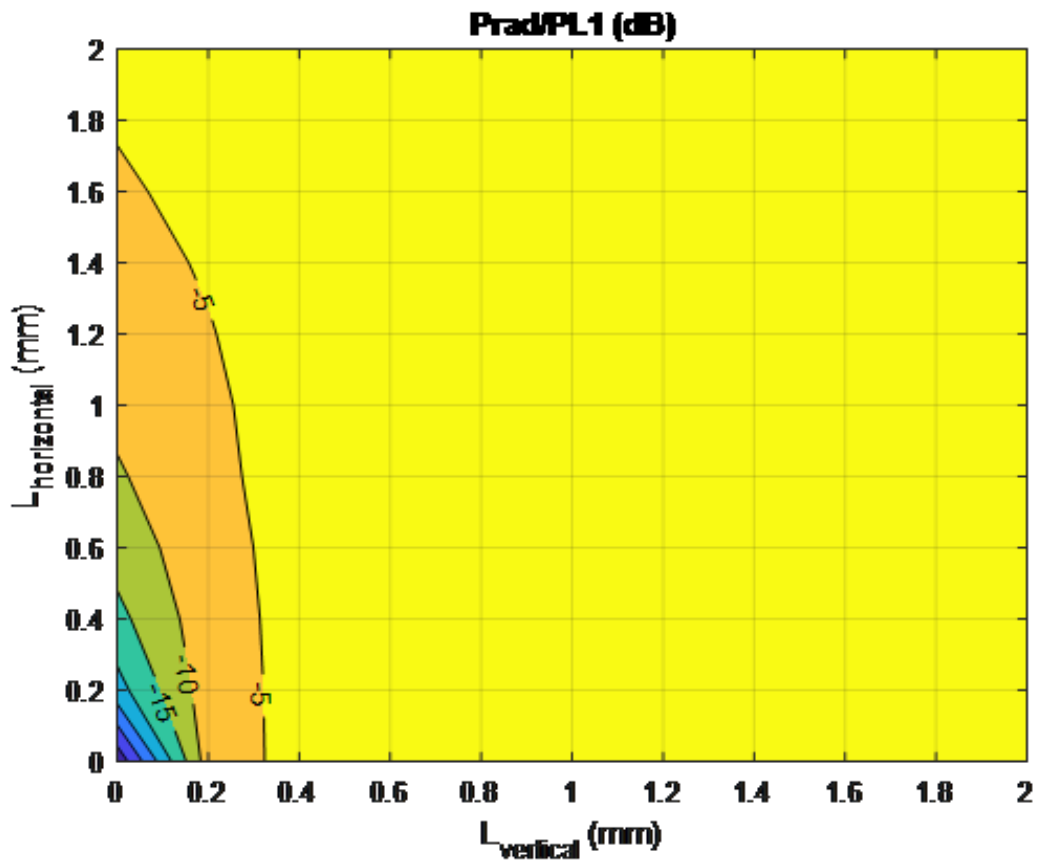

Figure 44: Variation of Q_u factor

Figure 45: Variation of radiated power $\frac{P_r}{P_{L1}}$ for different misalignments

As we can appreciate in figure (47), the wider the vertical cut is, the greater distance we obtains. We can conclude that the distance between the first and second resonant modes depend on the ratio width-length of the cavity.
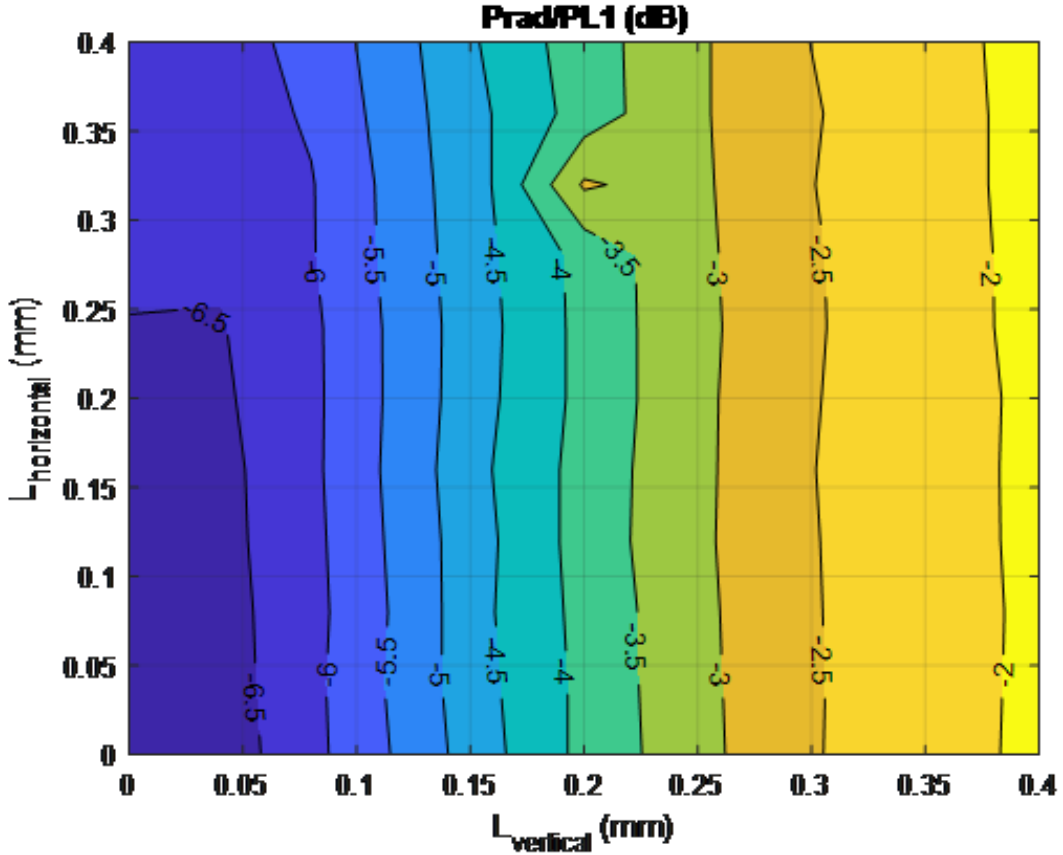
Figure 46: Variation of radiated power $\frac{P_r}{P_{L1}}$ for different misalignments

5.3 Alternated irises cavity

As well as we did with the inductive irises design, we are going to combine both ideas, mechanically tunable cavities and alternated irises cavity. Before obtaining any result and see the behaviour of different parameters, we need to see how to design the tunable structure. First of all, let's see what would happen if we introduce a vertical cut in the entire structure as we did in the previous design. Figures (48a) and (48b) show the outside and inside appearance in simulations of the structure with alternated couplings and vertical cut. The gap is defined as a vacuum brick with the same length and high than the whole structure.

As well as in the alternated system described in section 3, the mode which couples to axions is the fourth. In this structure, unlike the inductive system, the Ey-field is not constant, especially in the capacitive irises and surroundings. Additionally the surface current is not zero in the area of the vertical cut, which means that the electric field will scape from the structure. This increment in the radiated power will cause a dramatic decrease in the geometric factor C, and consequently, in the figure of merit F.O.M. For instance, for a gap length of 0.5mm we get a C factor of 0.00059295 and a F.O.M of 3.80359×10^{-12}. Moreover, the Scattering parameters are represented in figure 49, as we can appreciate, the transmitted power is practically zero, so that the
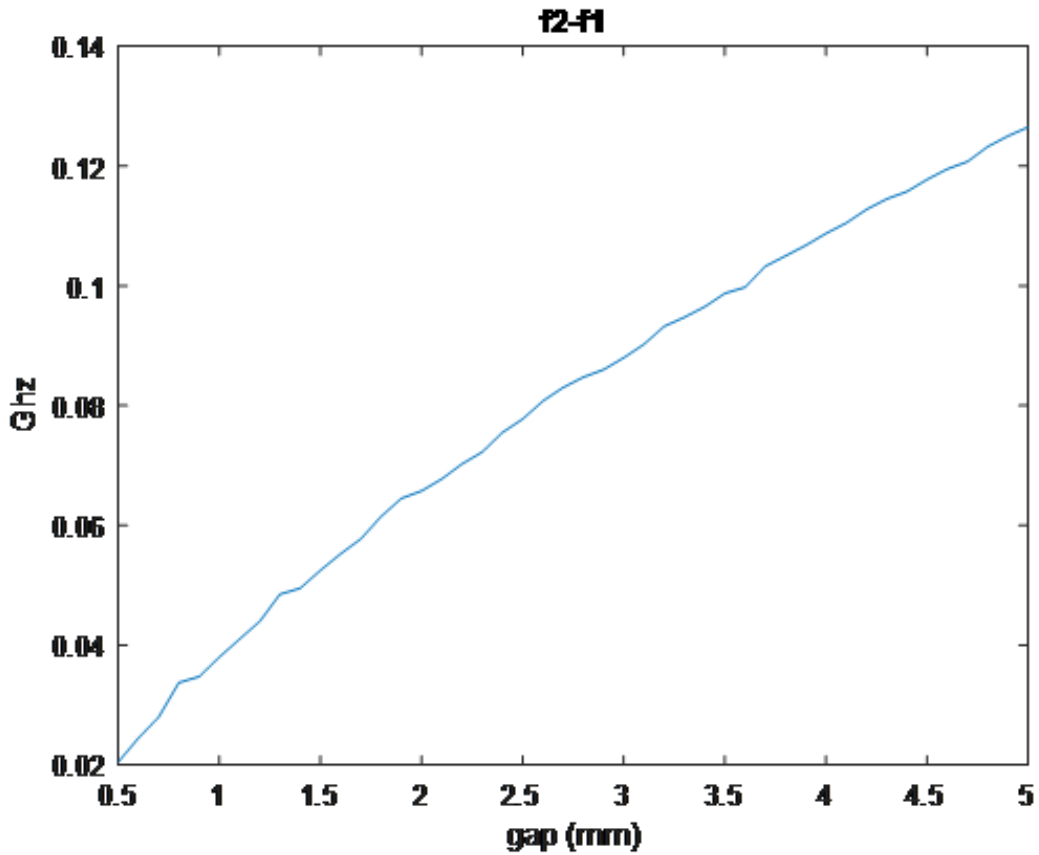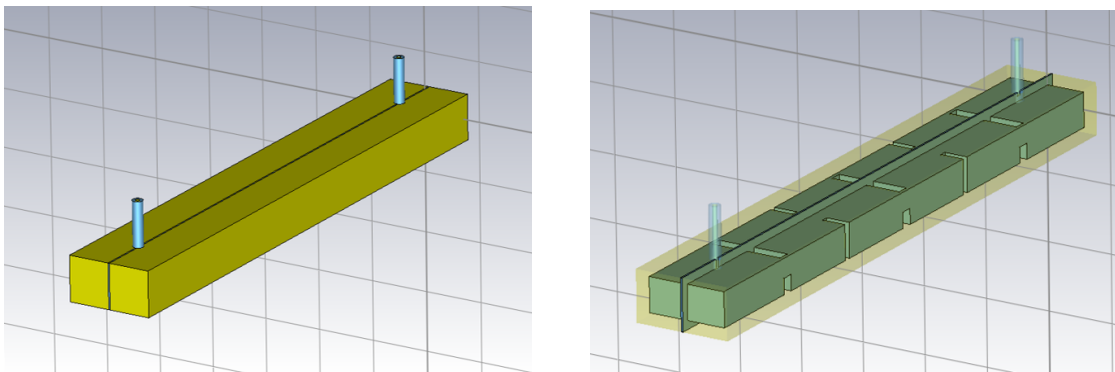
Figure 47: Variation of radiated power $\frac{P_r}{P_{L1}}$ for different misalignments

(a) CST design of alternated irises cavity with vertical cut

(b) CST design of alternated irises cavity with vertical cut

radiated power must have such a high value that it makes this design infeasible.

A solution for the mechanical tuning in the alternated design could be solved by introducing the vertical cut in the whole structure except for the capacitive irises, minimising the radiated losses. The idea consists on designing a structure in which the capacitive irises keep a physical contact independently of the vertical gap. Although the structure can be simulated easily, manufacturing this design could be a challenge.
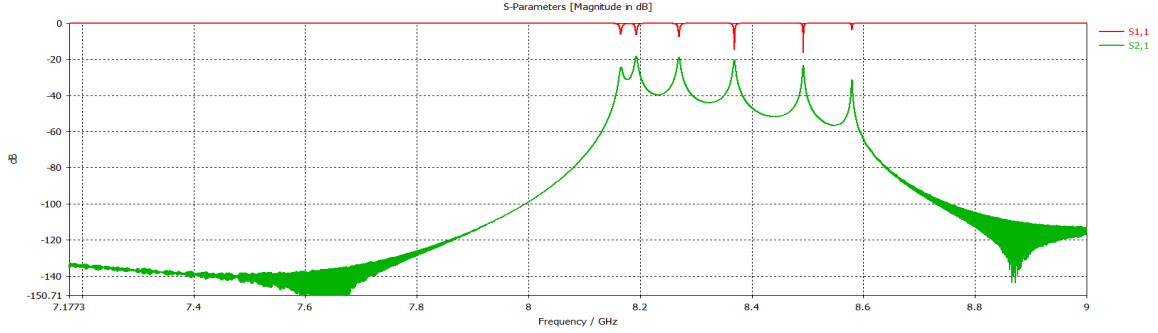
S-Parameters [Magnitude in dB]

Figure 49: Scattering parameters of the alternated irises cavity with vertical cut, separation of 0.5mm

In this section, we only focus on the theoretical simulations in order to see if the design is feasible and the behaviour of the same parameters than in the inductive irises cavity.

The appearance of the structure is displayed in figure 50a and 50b. Unlike the previous design, now the gap is defined as four vacuum bricks, separated by the capacitive irises. Additionally, the capacitive couplings play a alignment function in both directions, vertical and horizontal, so there is no sense in calculate the radiated losses due to geometric misalignment.
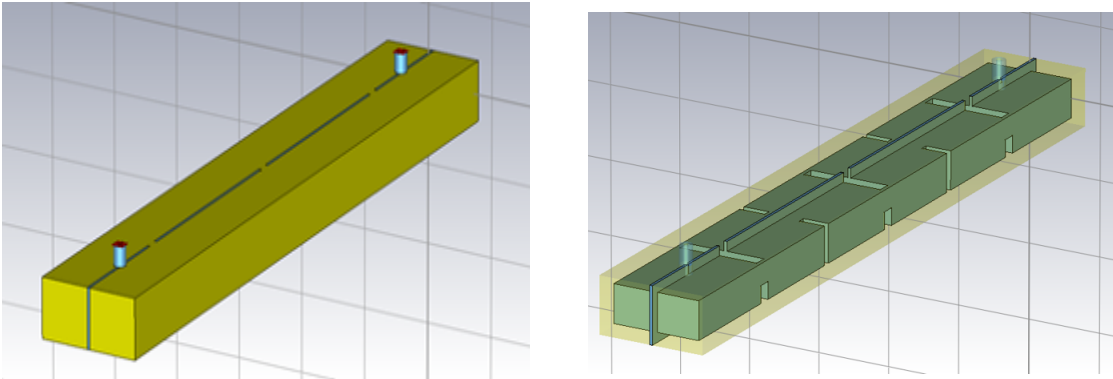
(a) CST design of alternated irises cavity with vertical cut

(b) CST design of alternated irises cavity with vertical cut

As we can see in figure 51, we get a frequency range of 400MHz for the same gap variation than in the inductive design, a range a bit smaller, 400 vs 700 MHz. Note that we are comparing the variation of the first resonant mode in the inductive designs with the variation of the fourth resonant mode in the alternating coupling design.

As well as we did in the inductive cavity design, we are going to calculate the variation of the inter-cavities factor, for the inductive and the capacitive couplings. As we have explained previously, the k factor for inductive irises is negative, whereas for
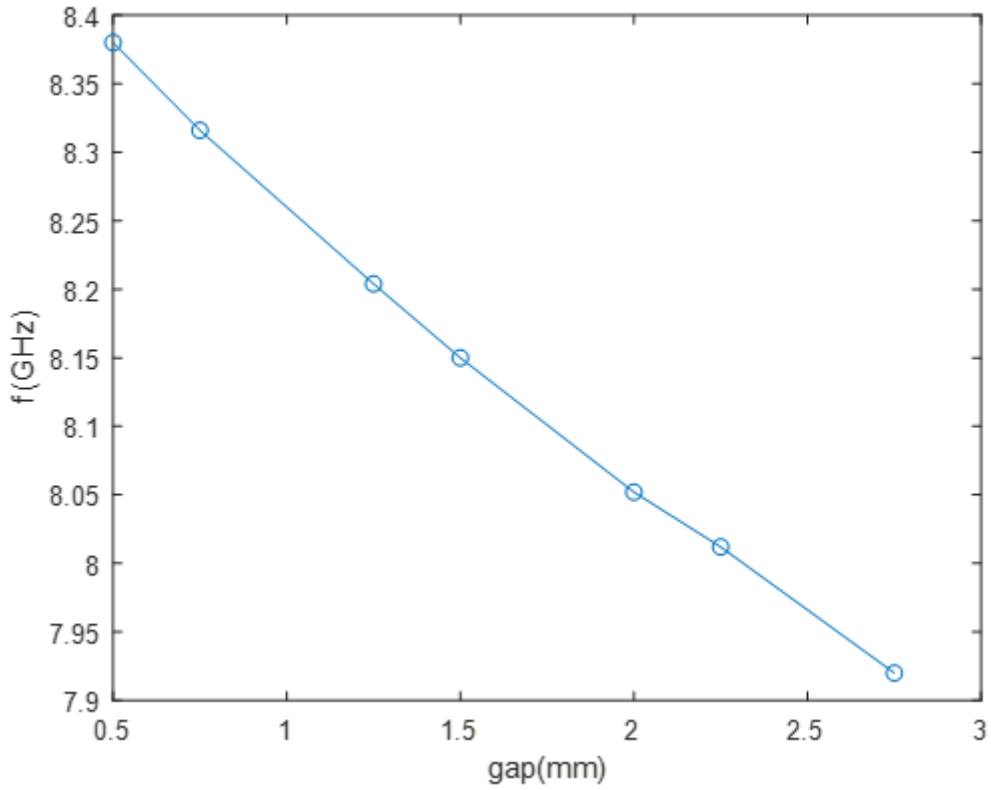
46

Figure 51: Frequency variation of the fourth resonant mode in the alternating tunable cavity

capacitive irises the k factor is positive. In order to make a comparison between both cases, we show in figure (52) the absolute value of the inductive irises.

We can observe in figure 52 that the variation of k factor in the inductive case is greater than for the capacitive irises.

Yet another parameter to study is the radiated power. Using the same procedure than in the inductive tunable cavity we obtain the result shown in figure (53). The radiated power is not relevant for a gap range to 3mm, we obtain less radiated power than in the whole inductive structure since contact is kept in the capacitive irises.
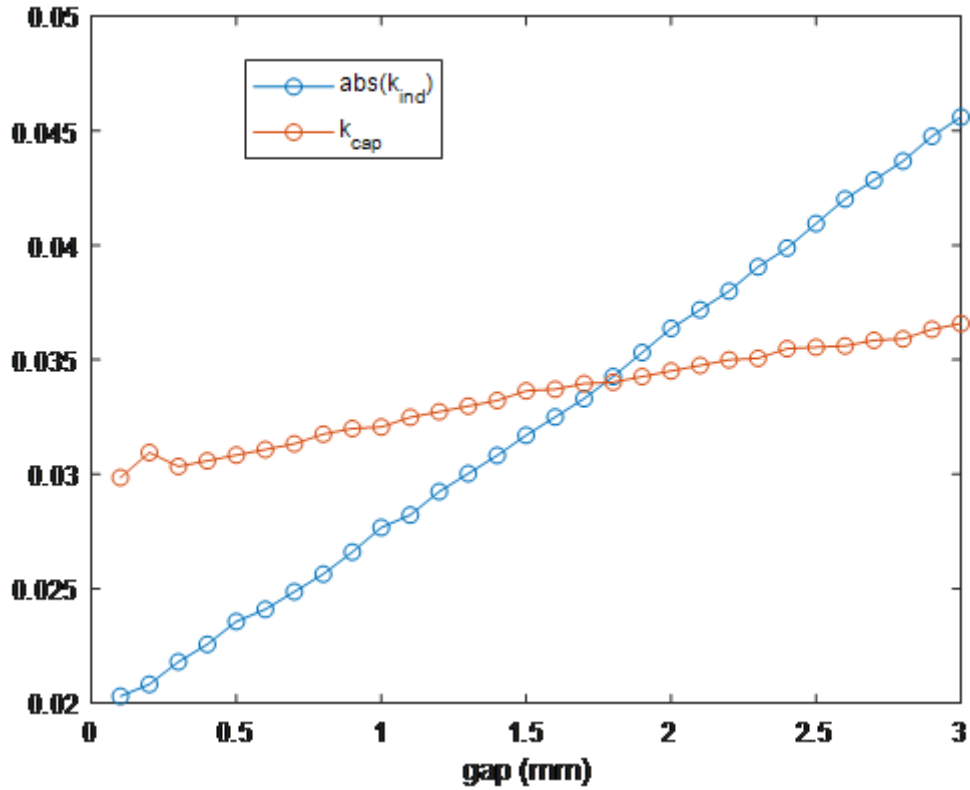
Figure 52: Frequency variation of the fourth resonant mode in the alternating tunable cavity

5.4 Pros and cons of tunable structures

this first design is a mere prototype. We have to spend more time searching new forms of developed the frequency tunable cavity. In this part, we have used a 20 inductive cavities for the simulation. For the alternated (capacitive and inductive) coupling, we can not apply this idea because of the electromagnetic field could scape from the system as soon as we do the vertical cut. We are developing new ideas for that challenge like make a tunable cavity varying the dielectric of it.
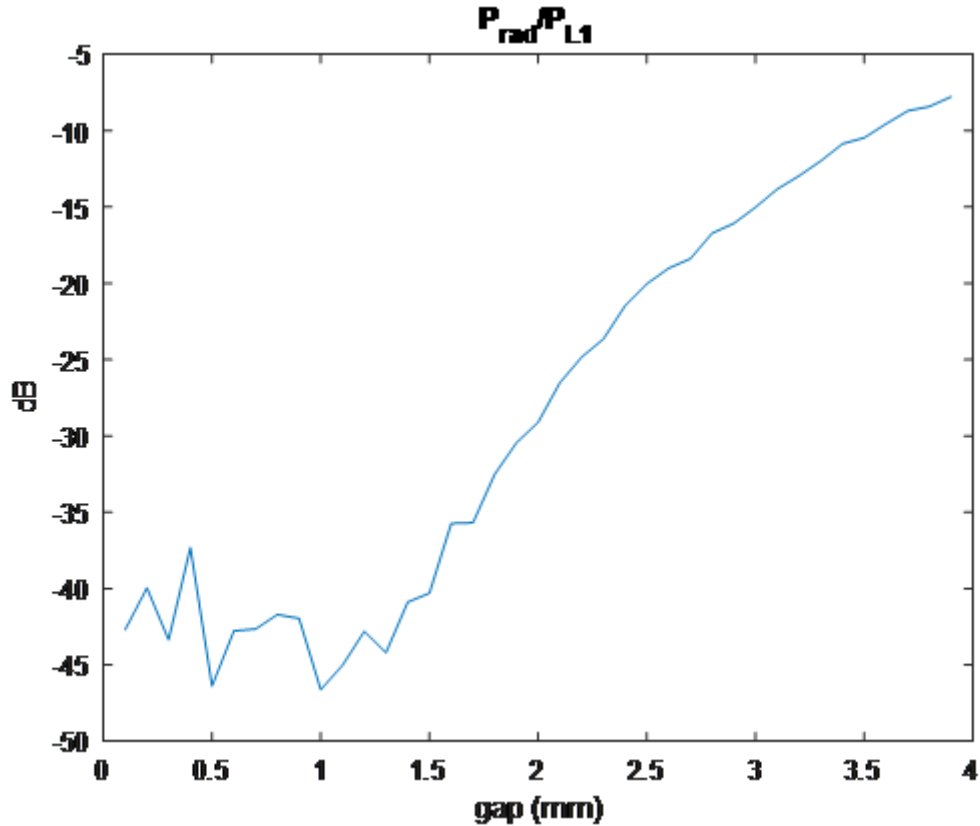
Figure 53: Frequency variation of the fourth resonant mode in the alternating tunable cavity

6   Conclusion and future lines

The work presented in the master thesis has been structured in order to achieve the main goal. We have successfully designed and manufactured a mechanical tunable system as well as an alternating coupled structure. Both devices are being physically studied at CERN, where they can be analysed at cryogenic temperature. Additionally, a larger alternating system is being manufactured also at CERN. This design presents enough volume to search axions taking into account nowadays models. Although the resonant frequency of this cavity is located inside the hypothetical axions region, the possibility to find the axion is low. However, it is a great opportunity to test the post processing part and check the potential for next iterations.

The simulation and manufacturing of the design with such characteristics have been a complete challenge. Not only caused by the complexity, but also for the size. More-over, simulations must present a high accuracy at room and at cryogenic temperature, increasing the time cost of each simulation. The time frame for the optimization process of the final thirty sub-cavities design was two weeks.

One of the most gratifying parts of this project becomes when the theoretical model and simulations agrees with the real measurements in the laboratory. This is the moment when we realise that everything we have calculated is correct.

Although we have advanced quite a lot in the project, we are in the middle of the project age and the are is still a lot of work to be done. Since creating larger structures is practically infeasible, we can focus our efforts in mainly two directions, new tunable systems and more stable structures.

Although it is not a big deal to simulate tunable mechanical cavities, manufacturing the tunable device is a challenge, even more at cryogenic temperature and in the presence of a 9 Tesla magnetic field. To cope with that problem, a suitable solution could be working with tunable electrical structures. Then, instead of modifying the frequency through the cavity geometry, we can vary it changing the internal material permittivity.

Another point consists of stablishing zeros at some specific frequencies so that we obtain a frequency spectrum with just one resonant mode. The main problem is how to combine this concept with a tunable system.

There are several problems when working with large structures, they are too complicated and we have many problems regarding with the tolerances. A solution could be the use of a certain amount of smaller cavities and combine them via hybrids. Although each cavity will have some variation in the resonant mode, we can stablish some zeros and with a fine tuning synchronise their frequency resonant mode.

References

[1] R. J. Cameron and Chandra M. Kudsia and Raafat R. Mansour, Microwave Filters for Communication Systems, 2007, Wiley, ISBN: 978-0-471-45022-1, Hoboken, New Jersey.

[2] A. Alvarez Melcon, Sergio Arguedas, Cristian Cogollos, et. al., "Axion Searches with Microwave Filters: the RADES project". Journal of Cosmology and Astroparticle Physics. $JCAP_017P_0318, April 2018, pp.1 - 23$.

[3] R. Peccei and H. R. Quinn,"CP conservation in the presence of instantons," $Phys.Rev.Lett.38(1977)1440 - 1443$.

[4] R. Peccei and H. R. Quinn, "Constraints imposed by CP conservation in the presence of instantons," $Phys.Rev.D16(1977)1791 - 1797$.

[5] P. Sikivie, "Experimental tests of the invisible axion," $Phys.Rev.Lett.51(1983)1415$.

[6] S. Asztalos, et. al. "Large-scale microwave cavity search for dark-matter axions", Physical Review D, Vol.64, 2001.

[7] P.Navarro "Investigaciones en un sistema de detección de axiones de materia oscura en microondas".

[8] David M. Pozar, "Analysis and Design of Cavity Coupled Microstrip Coupers and Transitions", IEEE Microwave Theory and Techniques, Vol. 51, No. 3, March 2003, pp.1034-1044.

[9] Tatsuo Itoh, "Periodic Structures for Microwave Engineering"

[10] J.Redondo "Axion D.M. cavity calculation"

[11] José Antonio Lorente Acosta, Alejandro Álvarez Melcón and Christoph Ernst, "Techniques for Loss Reduction in Waveguide Filters"

[12] David M. Pozar, "Microwave Engineering".

[13] Jia-Sheng Hong, M. J. Lancaster, "Microstrip Filters for RF/Microwave Applications"

[14] B.M. Brubaker, L. Zhong, S.K. Lamoreaux, K.W. Lehnert and K. A. Bibber, "The HAYSTAC Axion Search Procedure", June 27,2017.

[15] David M. Pozar, "Analysis and Design of Cavity Coupled Microstrip Coupers and Transitions", IEEE Microwave Theory and Techniques, Vol. 51, No. 3, March 2003, pp.1034-1044.

[16] http://www.cv.nrao.edu/course/astr534/Radiometers.html

[17] https://www.copper.org/resources/properties/cryogenic/